PLOS GENETICS

RESEARCH ARTICLE

TM2D genes regulate Notch signaling and neuronal function in *Drosophila*

Jose L. Salazar[1,2], Sheng-An Yang[1,2], Yong Qi Lin[3], David Li-Kroeger[2,4,5], Paul C. Marcogliese[1,2], Samantha L. Deal[2,6], G. Gregory Neely[3], Shinya Yamamoto[1,2,5,6,7,8]*

1 Department of Molecular and Human Genetics, Baylor College of Medicine (BCM), Houston, Texas, United States of America, **2** Jan and Dan Duncan Neurological Research Institute, Texas Children's Hospital, Houston, Texas, United States of America, **3** The Dr. John and Anne Chong Lab for Functional Genomics, Charles Perkins Centre and School of Life and Environmental Sciences, The University of Sydney, Sydney, Australia, **4** Department of Neurology, BCM, Houston, Texas, United States of America, **5** Center for Alzheimer's and Neurodegenerative Diseases, BCM, Houston, Texas, United States of America, **6** Program in Developmental Biology, BCM, Houston, Texas, United States of America, **7** Development, Disease Models & Therapeutics Graduate Program, BCM, Houston, Texas, United States of America, **8** Department of Neuroscience, BCM, Houston, Texas, United States of America

* yamamoto@bcm.edu

OPEN ACCESS

Citation: Salazar JL, Yang S-A, Lin YQ, Li-Kroeger D, Marcogliese PC, Deal SL, et al. (2021) *TM2D* genes regulate Notch signaling and neuronal function in *Drosophila*. PLoS Genet 17(12): e1009962. https://doi.org/10.1371/journal.pgen.1009962

Editor: Fengwei Yu, National University of Singapore, SINGAPORE

Received: May 10, 2021

Accepted: November 23, 2021

Published: December 14, 2021

Data Availability Statement: All relevant data are within the manuscript and its Supporting Information files.

Funding: This work was supported by the National Institutes of Health (RF1AG071557), Alzheimer's Association New Investigator Research Grant (NIRG-15-364099) and Nancy Chang, Ph.D. Award for Research Excellence to S.Y. J.L.S was supported by a training grant T32GM008307 from the National Institutes of Health. P.C.M. is supported by the Canadian Institutes of Health

Abstract

TM2 domain containing (TM2D) proteins are conserved in metazoans and encoded by three separate genes in each model organism species that has been sequenced. Rare variants in *TM2D3* are associated with Alzheimer's disease (AD) and its fly ortholog *almondex* is required for embryonic Notch signaling. However, the functions of this gene family remain elusive. We knocked-out all three *TM2D* genes (*almondex*, *CG11103/amaretto*, *CG10795/biscotti*) in *Drosophila* and found that they share the same maternal-effect neurogenic defect. Triple null animals are not phenotypically worse than single nulls, suggesting these genes function together. Overexpression of the most conserved region of the TM2D proteins acts as a potent inhibitor of Notch signaling at the γ-secretase cleavage step. Lastly, Almondex is detected in the brain and its loss causes shortened lifespan accompanied by progressive motor and electrophysiological defects. The functional links between all three *TM2D* genes are likely to be evolutionarily conserved, suggesting that this entire gene family may be involved in AD.

Author summary

Alzheimer's disease (AD) is the most common neurodegenerative disease affecting the aging population. Although many genetic factors have been implicated in its pathogenesis, *in vivo* functions of many of these genes have not been well defined. In this study, we investigated the function of *TM2D3*, a conserved gene that has been implicated in late-onset AD through an exome-wide association study, and two closely related genes, *TM2D1* and *TM2D2*, using the fruit fly *Drosophila melanogaster*. In addition to exhibiting a previously reported maternal-effect neuurodevelopmental phenotype caused by Notch signaling defects during embryogenesis, fly *TM2D3* mutants are short lived and display

Research (MFE-164712). Confocal imaging performed in this study was supported by the Eunice Kennedy Shriver Intellectual and Developmental Disabilities Research Center (IDDRC) at Baylor College of Medicine (P50HD103555). The funders had no role in study design, data collection and analysis, decision to publish, or preparation of the manuscript.

Competing interests: The authors have declared that no competing interests exist.

age-dependent motor and electrophysiological defects, providing the first link between this gene and age-dependent neurological phenotypes. Furthermore, *TM2D1* and *TM2D2* knockout flies phenotypically mimic the loss of *TM2D3*. Triple knockout of all three *TM2D* genes resemble the single knockouts, suggesting that these genes likely function together. Together with functional data that implicates TM2D3 in a biological process that is liked to the γ-secretase, a protease that is involved in AD in addition to being required for proper Notch signaling, we propose that all three *TM2D* family genes may be involved in AD pathogenesis, which warrants further investigation through human genetics studies.

Introduction

Alzheimer's disease (AD) is the most common neurodegenerative disease affecting the aging population and accounts for the large majority of age-related cases of dementia [1,2]. AD is pathologically characterized by histological signs of neurodegeneration that are accompanied by formation of extracellular plaques and intra-neuronal tangles. Numerous studies have identified genetic factors that contribute to AD risk and pathogenesis [3]. Rare hereditary forms of AD are caused by dominant pathogenic variants in *APP (Amyloid Precursor Protein)*, *PSEN1* (*Presenilin 1*) or *PSEN2 (Presenilin 2)*. These three genes have been extensively studied using variety of experimental systems, and the resultant knowledge has led to greater understanding of how they contribute to the formation of extracellular plaques found in both familial and sporadic AD brains [4]. *PSEN1* and *PSEN2* are paralogous genes that encode the catalytic subunit of the γ-secretase, a membrane-bound intramembrane protease complex [5]. γ-secretase substrates include many type-I transmembrane proteins including APP as well as Notch receptors that play various roles in development and physiology [6,7].

While studies of genes that cause familial AD have been critical in providing a framework to study pathogenic mechanisms of this disorder, pathogenic variants in *APP* and *PSEN1/2* are responsible for only a small fraction of AD cases [8]. Familial AD can be distinguished from more common forms of AD because most patients with pathogenic *APP* or *PSEN1/2* variants develop AD before the age of 65 [early-onset AD (EOAD)]. The majority (>95%) of AD cases are late-onset (LOAD, develops after 65 years of age), sporadic and idiopathic in nature [9]. In these patients, it is thought that multiple genetic and environmental factors collaborate to cause damage to the nervous system that converges on a pathway that is affected by APP and PSEN1/2. To reveal common genetic factors with relatively small effect sizes, multiple genome-wide association studies (GWAS) have been performed and identified over 40 loci throughout the genome that confer increase risk to developing AD [3]. The most notable risk-factors are variant alleles in *APOE* [10]. Although the precise molecular mechanism by which different alleles of *APOE* increase or decrease the risk of AD has been extensively debated, a number of studies have proposed that this gene is involved in the clearance of toxic Aβ peptides [11]. A recent meta-analysis has also identified *ADAM10* (encoding a β-secretase enzyme that cleaves APP and Notch) as an AD associated locus [12], suggesting that genes involved in familial EOAD and sporadic LOAD may converge on the same molecular pathway. Functional studies of these and other newly identified risk factors for AD are critical to fully understand the etiology of this complicated disease that lack effective treatments or preventions.

We previously reported that a rare missense variant (rs139709573, NP_510883.2:p.P155L) in *TM2D3* (*TM2 domain containing 3*) is significantly (OR = 7.45, pMETA = $6.6x10^{-9}$) associated with increased risk of developing LOAD through an exome-wide association study in

collaboration with the CHARGE (Cohorts for Heart and Aging Research in Genomic Epidemiology) consortium [13]. This variant was also associated with earlier age-at-onset that corresponds to up to 10 years of difference with a hazard ratio of 5.3 (95% confidence interval 2.7–10.5) after adjusting for the common *ε4* allele of *APOE*. Although the function of this gene in vertebrates was unknown and this missense variant was not predicted to be pathogenic based on multiple variant pathogenicity prediction algorithms including SIFT [14], PolyPhen [15] and CADD [16], we experimentally demonstrated that p.P155L has deleterious consequences on TM2D3 function based on an assay we established using *Drosophila* embryos [13]. The *Drosophila* ortholog of *TM2D3*, *almondex* (*amx*), was initially identified based on an X-linked female sterile mutant allele (amx^1) generated through random mutagenesis [17]. Although homozygous or hemizygous (over a deficiency) amx^1 mutant females and hemizygous (over Y chromosome) males are viable with no morphological phenotypes, all embryos laid by amx^1 hemi/homozygous mothers exhibit severe developmental abnormalities including expansion of the nervous system at the expense of the epidermis [18,19]. This 'neurogenic' phenotype results when Notch signaling mediated lateral inhibition is disrupted during cell-fate decisions in the developing ectoderm [20,21]. By taking advantage of this scorable phenotype, we showed that the maternal-effect neurogenic phenotype of amx^1 hemizygous females can be significantly suppressed by introducing the reference human TM2D3 expressed under the regulatory elements of fly *amx*, but $TM2D3^{p.P155L}$ expressed in the same manner fails to do so [13]. This showed that the function of *TM2D3* is evolutionarily conserved between flies and humans, and the molecular function of *TM2D3* that is relevant to LOAD may also be related to Notch signaling. More recently, another rare missense variant (p.P69L) in this gene has been reported in a proband that fit the diagnostic criteria of EOAD or frontotemporal dementia [22], indicating that other *TM2D3* variants may be involved in dementia beyond LOAD.

TM2D3 is one of three highly conserved TM2 domain containing (TM2D) proteins encoded in the human genome. The two other TM2 domain-containing proteins, TM2D1 and TM2D2, share a similar protein domain structure with TM2D3, and each protein is encoded by a highly conserved orthologous gene in *Drosophila* that has not been functionally characterized (*CG10795* and *CG11103*, respectively) (**S1 Fig**). All TM2D proteins have a predicted N-terminal signal sequence and two transmembrane domains that are connected through a short intracellular loop that are found close to the C-terminus. Within this loop, there is an evolutionarily conserved DRF (aspartate-arginine-phenylalanine) motif, a sequence found in some G-protein coupled receptors that mediates their conformational change upon ligand binding [23]. The extracellular region between the signal sequence and first transmembrane domain is divergent in different species as well as among the three TM2D containing proteins. In contrast, the sequences of the two transmembrane domains as well as the intracellular loop is highly conserved throughout evolution as well as between the three TM2 domain containing proteins [24] (**S1 Fig**). The three proteins also have short C-terminal extracellular tails that are evolutionarily conserved within orthologs but vary among the three proteins (e.g. TM2D1 has a slightly longer C'-tail than TM2D2 and TM2D3). The molecular functions of these conserved and non-conserved domains of TM2D proteins are unknown.

Amx has been proposed to function at the γ-secretase cleavage step of Notch activation based on a genetic epistasis experiment performed previously [25]. Notch signaling activation is initiated by the binding of the Notch receptor to its ligands (Delta or Serrate in *Drosophila*) [26]. This induces a conformational change of Notch to reveal a cleavage site that is recognized by ADAM10 [encoded by *kuzbanian* (*kuz*) in *Drosophila*] [27]. Notch receptor that has undergone ADAM10 cleavage (S2 cleavage) is referred to as N^{EXT} (Notch extracellular truncation) and becomes a substrate for γ-secretase [28]. N^{EXT} that is cleaved by γ-secretase (S3 cleavage) releases its intracellular domain (N^{ICD}), which then translocates to the nucleus and regulates

transcription of downstream target genes [29]. To determine how *amx* regulates Notch signaling, Michellod and Randsholt attempted to suppress the embryonic neurogenic phenotype of embryos produced from amx^{1} mutant mothers by zygotically overexpressing different forms of Notch using a heat-shock promoter [25]. While N^{ICD} was able to weakly suppress the neurogenic defect, N^{EXT} was not able to do so, suggesting that Amx somehow modulates the cleavage step that invovles the γ-secretase complex. However, because the phenotypic suppression observed by N^{ICD} in this study was very mild and since the authors used Notch transgenes that were inserted into different regions of the genome (thus N^{ICD} and N^{EXT} are likely to be expressed at different levels and cannot be directly compared), additional data is required to fully support this conclusion.

In this study, we generated clean null alleles of all three *Drosophila TM2D* genes using CRISPR/Cas9-mediated homology directed repair (HDR) and assessed their functions *in vivo*. Surprisingly, we found that *CG10795* (*TM2D1*) and *CG11103* (*TM2D2*) knockout flies are phenotypically indistinguishable from *amx* (*TM2D3*) null animals, displaying severe maternal-effect neurogenic phenotypes. We also generated double- and triple-knockout animals to determine whether these three genes have redundant functions in other Notch signaling dependent contexts during development. The triple-knockout of all *TM2D* genes did not exhibit any obvious morphological phenotypes but shared the same maternal-effect neurogenic phenotype similar to the single null mutants, suggesting these three genes function together. We also provide further evidence that Amx functions on γ-secretase to modulate Notch signaling *in vivo*, and further uncover a previously unknown role of this gene in the maintenance of neural function in adults.

Results

A clean null allele of *amx* fully recapitulates previously reported maternal-effect phenotypes

In a previous study, Michellod et al. reported the generation of a null allele of *amx* (amx^{m}) by generating flies that are homozygous for a deletion that removes *amx* and several other genes [*Df(1)FF8*] and bringing back a genomic rescue construct for *Dsor1*, an essential gene that lies within this locus [30]. The authors reported that zygotic amx^{m} [actual genotype: *Df(1)FF8; P* $(Dsor1^{+S})$] mutant flies have reduced eye size and nicked wing margin as adults, which are phenotypes that had not been reported in the classic amx^{1} allele. Because the amx^{1} allele is caused by a 5bp deletion that may still produce a product that encodes a portion of the N'-extracellular domain (*amx* is a single exon gene in *Drosophila*, hence will not be subjected to nonsense mediated decay), the authors concluded that amx^{1} is a hypomorphic allele.

Since *Df(1)FF8* has not been molecularly characterized and it was uncertain whether all of the phenotypes attributed to amx^{m} are due to loss of *amx* alone, we decided to generate a clean null allele of *amx* (hereafter referred to as amx^{Δ}) using CRISPR/Cas9 technology [31,32] (**Fig 1**). We knocked-in a dominant wing color marker (y^{wing2+}) to replace the coding sequence of *amx* using HDR [33] (**Fig 1A**). Insertion of this cassette was screened by the presence of the visible marker (dark wings) in a *yellow* mutant background and the targeting event was molecularly confirmed via Sanger sequencing. We also confirmed the loss of *amx* transcript by RT-PCR (**S2A Fig**). Similar to amx^{1}, homozygous amx^{Δ} females exhibit sterility and all embryos produced by these animals exhibit a neurogenic phenotype (**Fig 1C and 1D**). Both female fertility and neurogenic phenotypes of their progeny can be suppressed by introducing a 3.3 kb genomic rescue construct containing the *amx* locus **(Fig 1A, 1C and 1E)** [13]. Human TM2D3 expressed using the same regulatory elements has ~50% activity of fly Amx **(Fig 1C and 1G)**, consistent with what we previously observed using amx^{1} hemizygous females [13].

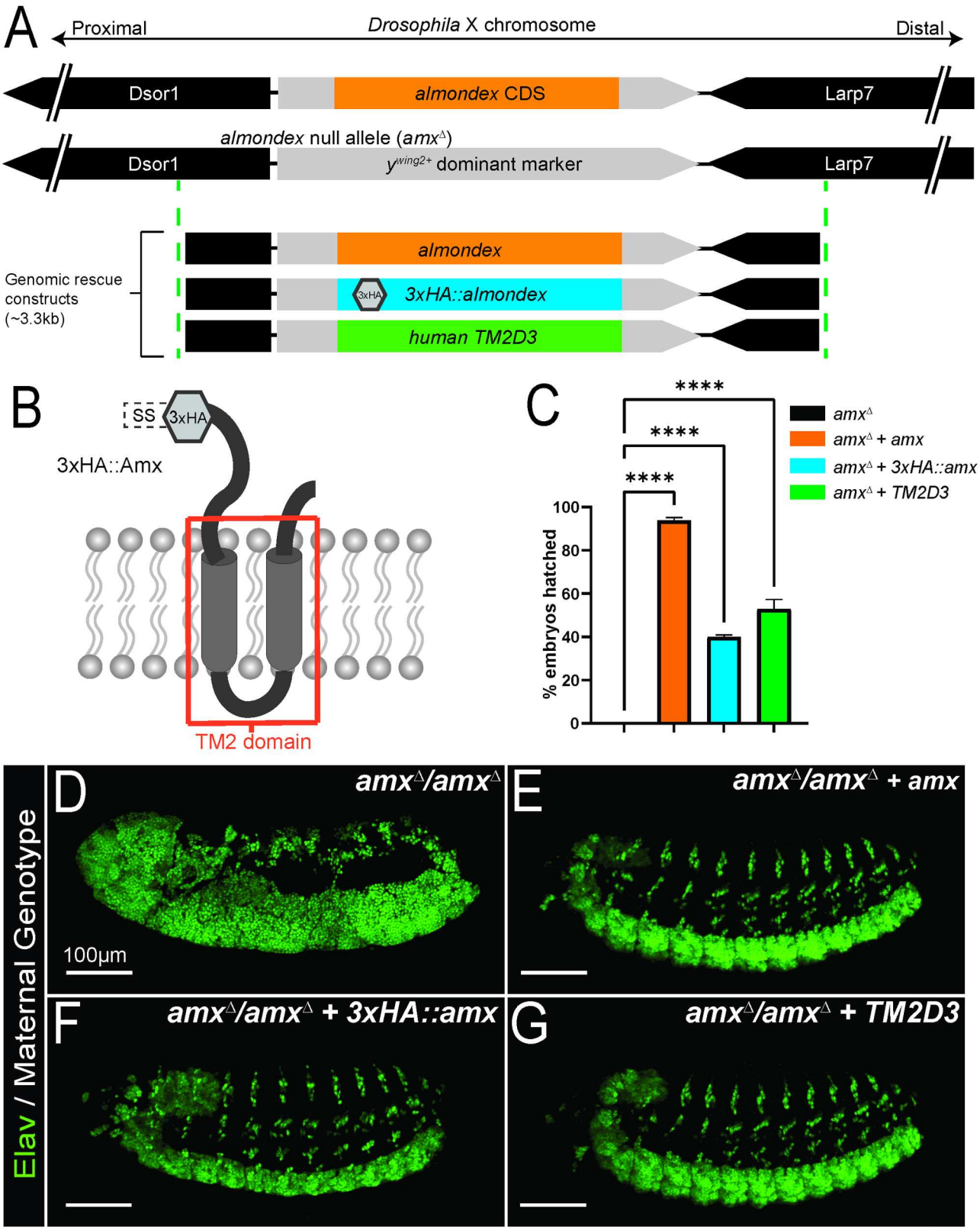

Fig 1. A clean null allele of *TM2D3* fly ortholog *almondex* (*amx*$^{\Delta}$) behaves like the classic *amx*^{1} allele. (A) Schematic diagram of *almondex* (*amx*) locus, *amx*$^{\Delta}$ allele and genomic rescue constructs used in this study. (B) Predicted 2D-structure of *Drosophila* Amx protein. SS = signal sequence for

membrane localization. Transmembrane 2 (TM2) domain is boxed in red. Hexagon denotes where 3xHA epitope is located in 3xHA::Amx protein. (C) Egg hatching assay shows that genomic rescue constructs can suppress embryonic lethality (amx^{Δ} n = 857. amx^{Δ} + *amx* n = 139. amx^{Δ} + *3xHA*::*amx* n = 1673. amx^{Δ} + *TM2D3* n = 257). Error bars show SEM. One-way ANOVA followed by Dunnett test. **** = p-value≤0.0001. (D-G) Embryonic nervous tissue (neuronal nuclei, Elav, green) of developing embryos. Embryos from homozygous amx^{Δ} females (D) exhibit a neurogenic phenotype. This phenotype can be suppressed by wild-type *amx* (E), *3xHA*::*amx* (F), or human *TM2D3* (G) genomic rescue constructs. Scale bars = 100 μm in (D-G).

https://doi.org/10.1371/journal.pgen.1009962.g001

We did not observe any morphological defects in the eye and wing of homozygous and hemizygous amx^{Δ} flies at all temperatures tested (between 18–29˚C). We also looked at other tissues that are often affected when Notch signaling is defective including the nota and legs [34,35] but we did not observe any morphological phenotypes in these tissues either. In summary, amx^{Δ} is the first clean loss-of-function (LoF) allele of *amx* generated by CRISPR/Cas9, and phenotypically resembles the classic amx^{1} allele rather than the amx^{m} allele.

Null alleles of other *TM2D* genes exhibit the maternal-effect neurogenic phenotype similar to *amx*

Using a similar strategy that we used to generate amx^{Δ} [33], we generated null alleles for *CG11103* (*TM2D2* ortholog, located on the X-chromosome) and *CG10795* (*TM2D1* ortholog, located on the 2nd chromosome), two uncharacterized genes without official names (**Fig 2**). This time, we inserted a dominant body color marker (y^{body+}) into the endogenous locus of *CG11103* or *CG10795* to individually knockout these genes (**Fig 2B and 2F**), and we phenotypically and molecularly characterized these alleles in a similar manner. We confirmed the loss of each transcript by RT-PCR (**S2A Fig**), confirming that the new lines we generated are true null alleles.

Both males and females that are hemizygous or homozygous null for *CG11103* are viable and these animals do not exhibit any morphological defects. Similar to *amx*, *CG11103* mutant females are fully sterile, and all embryos laid by these mothers exhibit neurogenic phenotypes (**Fig 2C**). Importantly, these phenotypes are rescued by a 1.5 kb genomic construct containing the *CG11103* locus (**Fig 2B, 2D and 2E**). Given the phenotypic and molecular similarities with *amx*, we gave *CG11103* the name *amaretto* (*amrt*), after the sweet Italian liqueur traditionally flavored with almonds. The knockout allele for this gene is referred to as $amrt^{\Delta}$ hereafter.

Like *amx* and *amrt*, mutants that are homozygous null for *CG10795* appear morphologically normal, but all females are sterile and their embryos exhibit a neurogenic phenotype (**Fig 2G**). We were able to suppress these phenotypes using a ~40kb fosmid transgene in which the CG10795 protein is C-terminaly tagged with multiple epitopes including GFP (**Fig 2F, 2H and 2I**) [36]. Given the phenotypic similarity to *amx* and *amrt* mutants, we named this gene *biscotti* (*bisc*), after the Italian biscuits traditionally made with almonds. The knockout allele for this gene is referred to as $bisc^{\Delta}$ hereafter and the fosmid-based GFP-tagged genomic rescue transgene is referred to as *bisc*::*GFP*.

Triple knockout of *TM2D* genes is phenotypically similar to single gene knockouts

The embryonic neurogenic defect is a rare phenotype that is almost exclusively associated with genes that affect the Notch signaling pathway [20]. Given the importance of Notch signaling in most stages of development preceding adulthood [7], it was peculiar that all three *TM2D* gene mutants do not exhibit any obvious developmental morphological defects related to Notch signaling while all three alleles exhibit a robust maternal-effect neurogenic phenotype. To test whether this may be due to redundancy between the three genes, we generated a fly strain that lacks all three *TM2D* genes (**Fig 3**).

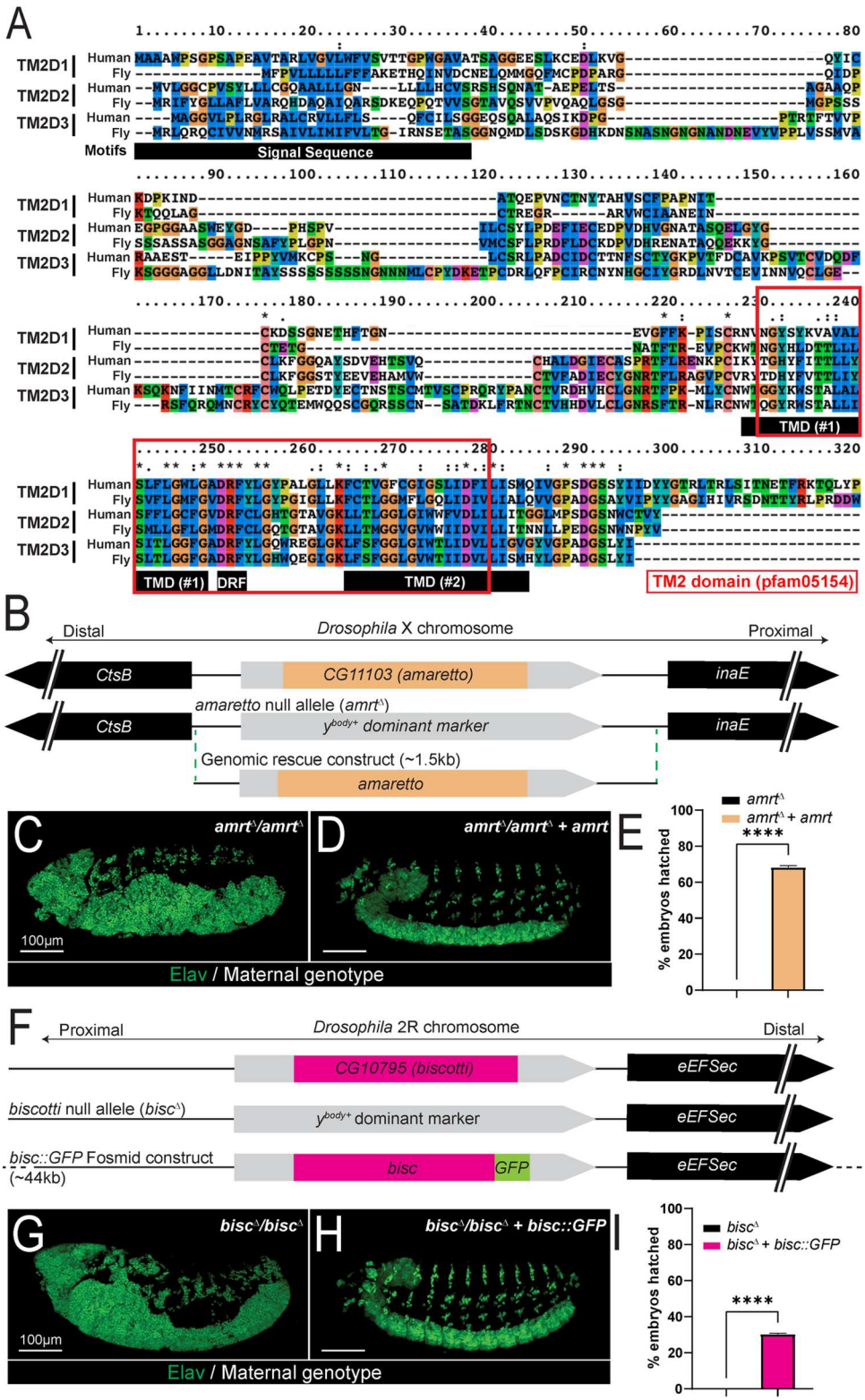

Fig 2. Null alleles of fly orthologs of *TM2D2* (*CG11103/amrt*) and *TM2D1* (*CG10795/bisc*) phenotypically mimics the loss of *TM2D3* (*amx*). (A) Protein alignment of human and *Drosophila* TM2D proteins. The TM2 domain (boxed in red) is composed of two transmembrane domains (TMD) and an intracellular DRF motif (denoted by black bars for TM2D3). (B) Schematic of *amaretto* (*amrt*) locus, *amrt* null allele ($amrt^{\Delta}$), and *amrt* genomic rescue plasmid construct

generated for this study. (C) Embryos from homozygous $amrt^{\Delta}$ females exhibit neurogenic phenotype, which can be suppressed by the *amrt* genomic rescue construct (D). (E) Egg hatching assay showing that *amrt* genomic rescue construct suppresses 68% of embryo lethality ($amrt^{\Delta}$ n = 954. $amrt^{\Delta}$ + *amrt* n = 1490). (F) Schematic of *biscotti* (*bisc*) locus, *bisc* null allele ($bisc^{\Delta}$), and *bisc*::*GFP* genomic rescue fosmid construct generated for this study. (G) Embryos from homozygous $bisc^{\Delta}$ females exhibit neurogenic phenotype (n = 379) which can be suppressed by *bisc*::*GFP* genomic rescue construct (H). (I) Egg hatching assay showing that *bisc*::*GFP* suppresses 30% of embryonic lethality ($bisc^{\Delta}$ n = 379. $bisc^{\Delta}$ + *bisc*::*GFP* n = 436). t-test, **** = p-value<0.0001. Scale bars = 100 μm in (C, D, G, H).

https://doi.org/10.1371/journal.pgen.1009962.g002

Because *amx* and *amrt* are both located on the X-chromosome (located in cytological regions 8D2 and 12C4, respectively, which are 19cM away), we recombined the two null alleles by following the dominant wing color and body color markers knocked into each locus (**Fig 3A**). The *amx*, *amrt* double null flies (amx^{Δ} $amrt^{\Delta}$) in a *yellow* mutant background exhibit wild-type color wings (y^{wing2+} marker of amx^{Δ}) and bodies (y^{body+} marker of $amrt^{\Delta}$). Absence of both *amx* and *amrt* transcripts in this line was verified by RT-PCR (**S2B Fig**). These double null adult flies also appeared morphologically normal similar to the single null animals (**Fig 3F, 3I and 3L**), suggesting that these two genes do not play redundant roles during the development of imaginal tissues. Consistent with single null animals, the *amx*, *amrt* double null females were fully sterile, exhibiting a maternal-effect neurogenic phenotype (**Fig 3C**).

We next combined the $bisc^{\Delta}$ allele on the second chromosome with the amx^{Δ} $amrt^{\Delta}$ mutant X-chromosome to generate a triple null mutant line (amx^{Δ} $amrt^{\Delta}$; $bisc^{\Delta}$) (**Fig 3A**). Absence of transcripts of all three *TM2D* genes in this line was verified by RT-PCR (**S2B Fig**). This genetic manipulation still did not produce any adult animals with obvious Notch signaling related external morphological defects (**Fig 3G, 3J and 3M**), suggesting that these three genes also do not play redundant roles in these contexts. Consistent with the single and double null lines, the triple null mutant females are also completely sterile and their progeny show maternal-effect neurogenic defects (**Fig 3D**). We did not observe any differences in the severity of the neurogenic phenotype in the embryos from the single gene knockouts and the triple knockout mothers (**Figs 1D, 2C, 2G and 3D**), likely because the neurogenic defect is already strong in single gene knockout animals, precluding any additive or synergistic effects.

According to large-scale transcriptomic studies, mRNA of *amx*, *amrt* and *bisc* are expressed relatively ubiquitously with some enrichment found in the female ovary [37,38]. Within the ovary, these three genes are likely to be expressed in similar cell types including germline cells and follicle cells according to a large single cell RNA-sequence database that have recently been released on the *bioRxiv* preprint server [39]. To further test whether *amx*, *amrt* and *bisc* do not have overlapping functions, we assessed whether genomic rescue transgenes for *amrt* or *bisc* can rescue *amx* mutants. If TM2D family proteins perform similar molecular tasks, increased expression of one gene is expected to suppress the LoF phenotype of another gene. Homozygous amx^{Δ} female flies with *amrt* or *bisc*::*GFP* genomic rescue transgenes (used to rescue $amrt^{\Delta}$ and $bisc^{\Delta}$ in **Fig 2**, respetively) are fully sterile, demonstrating that *amrt* or *bisc* are not able to substitute for the loss of *amx*. Together with our earlier finding that single *TM2D* gene knockout flies are phenotypically indistinguishable (**Figs 1 and 2**), and that no further phenotype or exacerbation is seen in the triple null mutant line (**Fig 3**), we conclude that these three genes are uniquely maternally required during embryonic neurogenesis and likely function together.

A truncated but not the full length form of Amx acts as a potent inhibitor of Notch signaling

Knockout experiments revealed that each of the three *TM2D* genes are individually maternally necessary for proper Notch signaling during embryogenesis, while being dispensable for other

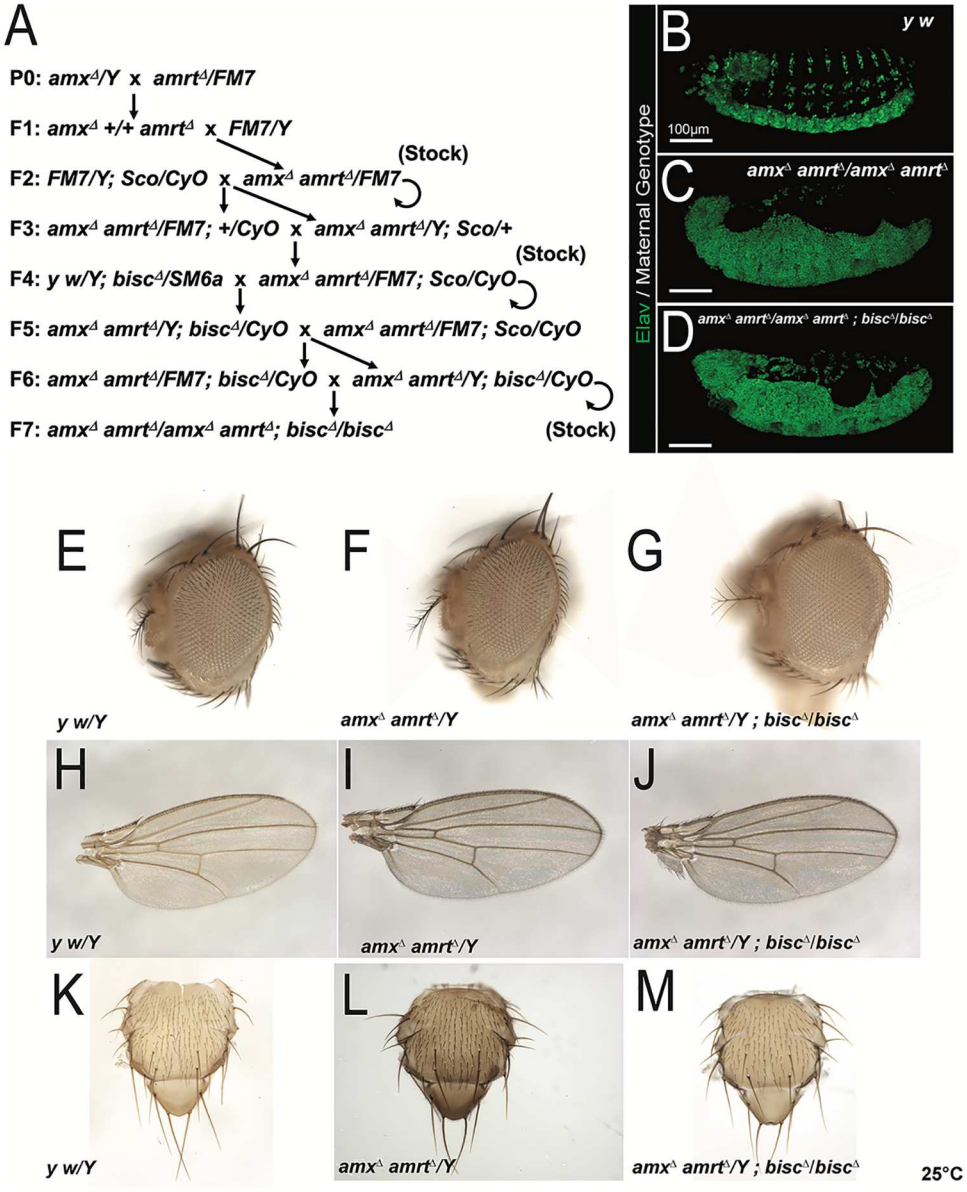

Fig 3. Triple null mutant for all three *TM2D* fly genes is phenotypically similar to single null mutants. (A) Crossing scheme used to generate *TM2D* triple null mutant flies. (B) A normal embryonic nervous system highlighted by neuronal nuclei marker Elav (green). (C-D) amx^{Δ} $amrt^{\Delta}$ double mutants (C) and amx^{Δ} $amrt^{\Delta}$ $bisc^{\Delta}$ triple mutants (D) exhibit a neurogenic phenotype. (E-K) *TM2D* double and triple null mutants exhibit no overt morphological phenotypes. Head structures of mutants (F, G) appear normal compared to *y w* control (E). Mutant wings (I, J) and thorax (L, M) also appear normal compared to control (H, K). Scale bars = 100 μm in (B-D).

https://doi.org/10.1371/journal.pgen.1009962.g003

developmental contexts that are known to depend on Notch. To further study the function of TM2D proteins *in vivo*, we tested whether overexpression of Amx is sufficient to modulate Notch signaling (Fig 4). In addition to generating transgenes that allow the expression of a full-length Amx protein with or without an N'-3xHA tag (placed immediately after the predicted signal sequence, 3xHA::Amx^{FL}) (Fig 4A) using the GAL4/UAS binary expression system [40], we generated a version of the N'-3xHA tagged construct that lacks the majority of the non-conserved N'-terminal extracellular domain (3xHA::$Amx^{\Delta ECD}$) (Fig 4D) to specifically test the function of the highly conserved TM2 domain through overexpression experiments.

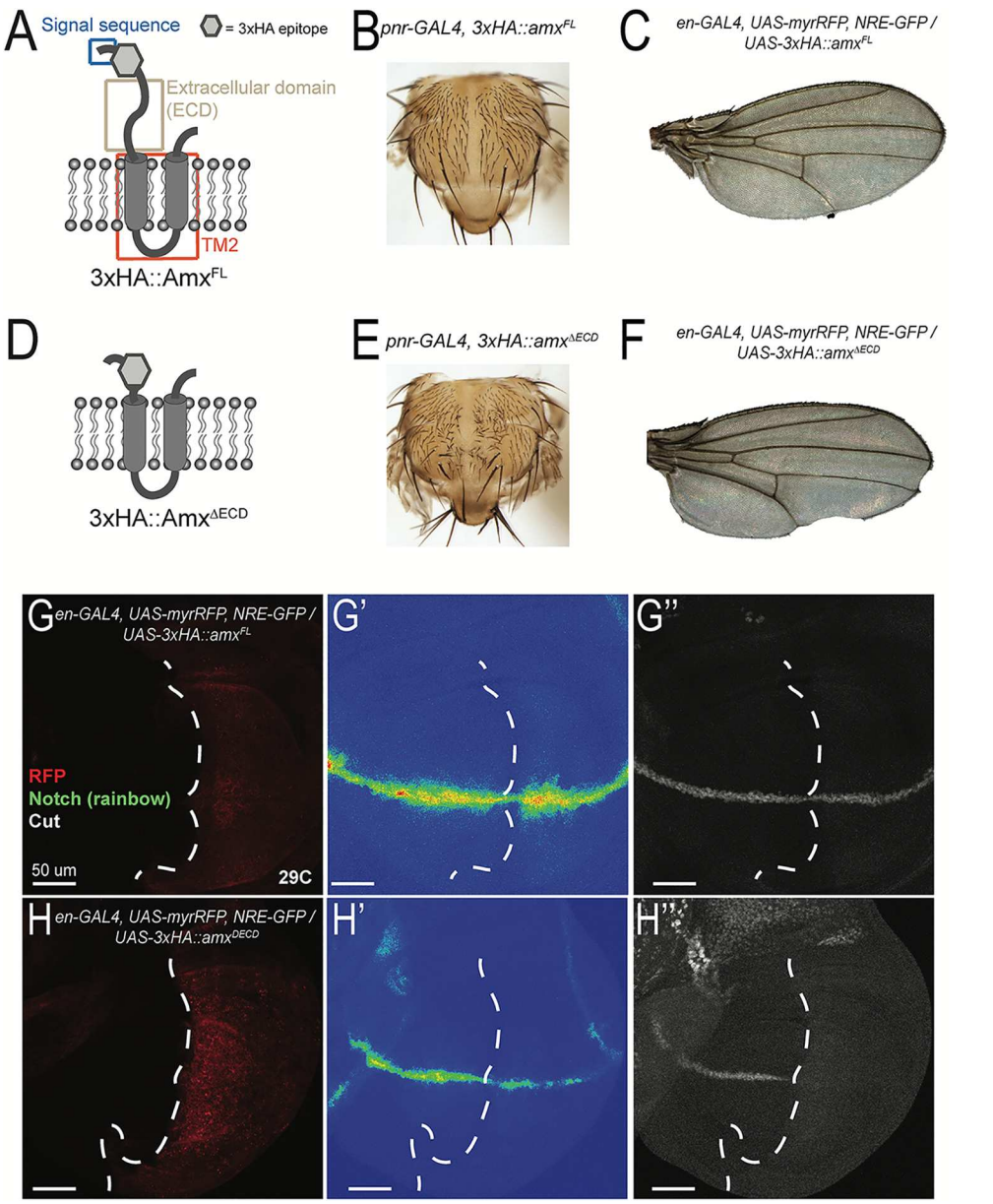

Fig 4. Amx that only possesses the highly conserved TM2 domain is a potent inhibitor of Notch signaling. (A, D) Schematic of proteins generated from *UAS-3xHA::amx*^{FL} and *UAS-3xHA::amx*$^{\Delta ECD}$ transgenes. A 3xHA epitope (grey hexagon) was inserted after a predicted signal sequence (SS, blue box). The majority of the extracellular domain (ECD, light brown box) was removed to generate 3xHA::amx$^{\Delta ECD}$, consisting mostly of the TM2 domain (red box) tagged with the N-terminal 3xHA epitope. (B) Overexpression of 3xHA::Amx^{FL} with *pannier(pnr)*-GAL4 has no effect on notum morphology. The absence of bristles along the midline is due to a very mild dorsal closure defect caused by the *pnr*-GAL4 insertion. (C) Expression of 3xHA::Amx^{FL} in the posterior wing using *engrailed* (*en*)-GAL4 has no effect of the morphology of wings of adults raised at 29˚C. (E) *pnr-GAL4* driven overexpression of truncated Amx causes an increase in the number of micro- and macrochaete, indicative of loss of Notch mediated lateral inhibition. (F) *en-GAL4* driven overexpression of 3xHA::Amx$^{\Delta ECD}$ causes notching of the posterior wing margin. (G-H) Immunostaining of wing imaginal discs expressing full-length or truncated 3xHA::Amx. (G) 3xHA::Amx^{FL} expression in the posterior imaginal wing disc using *en-GAL4* has no effect on NRE (Notch response element)-GFP expression, a synthetic *in vivo* Notch signaling reporter (G', rainbow) and on Cut (G", white) expression, a downstream target of Notch activation in this context. The domain expressing GAL4 is marked by RFP (red). (H) Expression of 3xHA::Amx$^{\Delta ECD}$ decreases NRE-GFP (rainbow) expression (H') and reduces Cut expression (H"). Scale bars = 50 μm in (G-H).

https://doi.org/10.1371/journal.pgen.1009962.g004

We first overexpressed these transgenes in the developing dorsal thorax using *pannier-GAL4* (*pnr-GAL4*). While we observed that Amx^{FL} does not cause any morphological defects (Fig 4B), we found that $Amx^{\Delta ECD}$ causes an increase in the number of mechanosensory bristles (Fig 4E), suggesting an effect on Notch mediated lateral inhibition. We then expressed the two proteins in the developing posterior compartment within wing imaginal discs using *engrailed-GAL4* (*en-GAL4*). We observed notching of the posterior wing margin when $Amx^{\Delta ECD}$ was expressed (Fig 4F), while no such defect was seen upon expression of Amx^{FL} (Fig 4C). To determine whether the wing notching caused by $Amx^{\Delta ECD}$ overexpression was indeed due to loss of Notch signaling, we visualized Notch activation using *NRE-GFP* (*Notch Responsive Element-Green Fluorescent Protein*), a synthetic *in vivo* Notch signaling reporter [41], as well as immunostaining of Cut, encoded by an endogenous downstream target gene of Notch activation in this context [42]. While overexpression of Amx^{FL} did not affect *NRE-GFP* and Cut expression (Fig 4G–4G"), $Amx^{\Delta ECD}$ caused a reduction in both *NRE-GFP* and Cut expression within the *en-GAL4* expression domain (Fig 4H–4H"). In summary, overexpression of full-length Amx did not affect developmental events related to Notch signaling in the thorax and wing, while overexpression of a truncated form that only carries the conserved TM2 domain and its short C'-tail inhibited Notch signaling in several developmental contexts.

Truncated Amx inhibits Notch signaling at the γ-secretase mediated receptor cleavage step

To determine how $Amx^{\Delta ECD}$ inhibits Notch signaling when ectopically overexpressed, we performed similar epistasis experiments as [25], but with improved genetic tools (Fig 5). First, we generated several new UAS constructs expressing different forms of Notch and inserted them into the identical genomic location on the 2nd chromosome using site specific ϕC31-mediated transgenesis to avoid positional effects [43,44] (Fig 5A). In addition to transgenes that allow expression of N^{ICD}, N^{EXT} and full-length Notch (N^{FL}), we also generated a ligand-independent form of *UAS-Notch* that still depends on ADAM10 and γ-secretase by deleting several epidermal growth factor-like repeats (EGF) of the extracellular domain that contains the ligand binding domain and Lin-12/Notch Repeats (LNR) within the negative regulatory region ($N^{\Delta EGF1\text{-}18.LNR}$) based on an earlier construct designed by [45]. When we overexpressed N^{ICD}, N^{EXT} or $N^{\Delta EGF1\text{-}18.LNR}$ in the developing wing pouch using *nubbin-GAL4* (*nub-GAL4*), we observed increased Cut expression throughout the wing pouch, indicating ectopic Notch activation (Fig 5B–5E and 5I). Over-expression of N^{FL} only showed a mild increase in Cut expression in limited regions of the wing pouch (S3A Fig), likely due to its ligand-dependence. These observations are consistent with previous reports using *UAS-Notch* transgenic lines generated using random (*P*-element mediated) transgenesis technology [46].

Next, we recombined *nub-GAL4* and *UAS-3xHA::amx*$^{\Delta ECD}$ onto the same chromosome. The resultant genetic recombinants constitutively overexpresses $Amx^{\Delta ECD}$ in the wing pouch, with heterozygous adults exhibiting wing notching and homozygous animals completely lacking wings in adulthood (S4A and S4B Fig). We then crossed these *nub-GAL4*, *UAS-3xHA::amx*$^{\Delta ECD}$ flies to different *UAS-Notch* lines to determine if $Amx^{\Delta ECD}$ can modulate the ectopic Cut expression phenotype caused by Notch overexpression. We found that co-overexpression of $Amx^{\Delta ECD}$ significantly suppresses the induction of Cut expression caused by $N^{\Delta EGF1\text{-}18.LNR}$ or N^{EXT} (Fig 5G–5I), but had no effect on the same phenotype caused by N^{ICD} (Fig 5F and 5I). This indicates that *amx*$^{\Delta ECD}$ genetically acts at the γ-secretase-mediated cleavage step of Notch activation, consistent with previous epistasis experiments performed in embryos using *amx*^{1} [25].

To further understand how $Amx^{\Delta ECD}$ inhibits Notch signaling upon overexpression, we assessed the distribution of the Notch receptor through immunostaining using a monoclonal

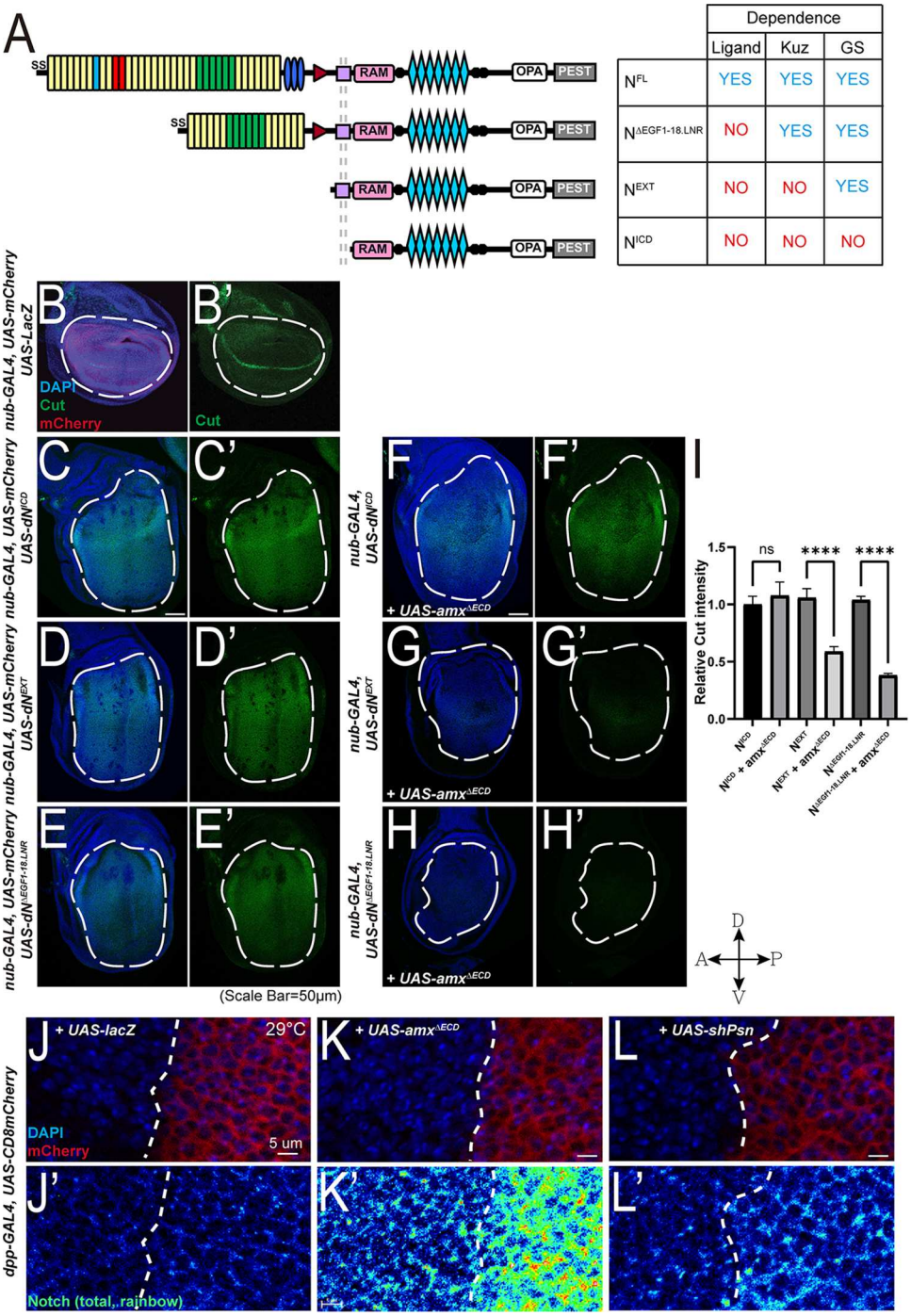

Fig 5. Genetic epistasis experiments place truncated Amx at the γ-secretase cleavage step of Notch activation. (A) Schematics and characteristics of Notch proteins made from each *UAS-Notch* transgenes that were generated for this study. Full-length Notch (N^{FL}) requires ligand binding and processing by Kuzbanian (Kuz) and γ-secretase (GS) for activation. Notch with EGF repeats and LNR domains removed ($N^{\Delta EGF1\text{-}18.LNR}$) is not dependent on ligands but are dependent on both Kuz and GS for activation. Notch with an extracellular truncation (N^{EXT}) is dependent only on GS for activation. The Notch intracellular domain (N^{ICD}) is constitutively active. (B) Cut (green) along the dorsoventral midline within the wing pouch [marked by *nub-GAL4 UAS-mCherry* (red), outlined by a white dash oval) is induced by Notch signaling. LacZ is expressed as a neutral protein. (C-E) Expression of Notch constructs leads to increase in Cut expression, quantified in (I). (F) Co-overexpression of 3xHA::$Amx^{\Delta ECD}$ has no effect of N^{ICD} mediated increases in Cut expression (F', I). (G-H) 3xHA::$Amx^{\Delta ECD}$ expression suppresses the effects of $N^{\Delta EGF1\text{-}18.LNR}$ and N^{EXT} on Cut expression (G', H', I). t-test. * = $p<0.05$. **** = $p<0.0001$. Error bars show SEM. (J-L) Overexpression of 3xHA::

$Amx^{\Delta ECD}$ causes an increase of Notch protein levels (K') compared to overexpression of a neutral protein, LacZ (β-galactosidase) (J'). Knockdown of *psn* mediated by shRNA also results in mild increase Notch levels (L'), mimicking the effect of 3xHA::$Amx^{\Delta ECD}$. DAPI marks nuclei of wing disc cells whereas mCherry labels the *dpp-GAL4* expression domain, the boundary of which is indicated by white dash lines, in J-L. Scale bars = 50 μm in (B-H). Scale bars = 5 μm in (J-L).

https://doi.org/10.1371/journal.pgen.1009962.g005

antibody that recognizes both cleaved and uncleaved forms of Notch [47]. Upon overexpression with *decapentaplegic-GAL4* (*dpp-GAL4*), which is expressed in a limited domain within the wing pouch, we observed that $Amx^{\Delta ECD}$ causes wing notching (**S4D Fig**) that is accompanied by a dramatic upregulation of Notch receptor (**Figs 5K–5K' and S5B**). Wing notching was not observed when Amx^{FL} was overexpressed (**S4C Fig**), consistent with the results obtained using *en-GAL4* and *nub-GAL4*. To test whether a similar phenotype is seen upon loss of γ-secretase function, we knocked down *Presenilin (Psn*, which is orthologous to human *PSEN1* and *PSEN2)* in the wing disc and assessed its effect on Notch protein levels. When we performed RNAi against *Psn* using a *UAS-RNAi* line that had been validated in a previous study [48] with *dpp-GAL4*, we found that knockdown of *Psn* shows an accumulation of Notch similar to $Amx^{\Delta ECD}$ over-expression but to a lesser extent (**Figs 5L–5L' and S5C**). Next, to determine if the Notch receptor was accumulating at the cell surface, we performed a detergent-free immunostaining using an antibody that recognizes the extracellular domain of the Notch receptor [49]. We found that the level of Notch present at the cell surface was increased upon overexpression of $Amx^{\Delta ECD}$ or *Psn* knockdown, however to a lesser extent compared to the total Notch staining (**S5D–S5F' Fig**). Therefore, Notch receptors seem to accmumulate both at the cell surface and in intracellular compartments in these contexts, suggesting a defect in protein trafficking or turnover. To also test whether this Notch accumulation phenotype occurs when Notch cleavage is altered by another mechanism, we tested whether loss of ADAM10 also causes this defect. When we generated mutant clones of a null allele of *kuz* (kuz^{e29-4}) [50] using MARCM (Mosaic analysis with a repressible cell marker) [51], we did not observe any alterations in Notch levels (**S6 Fig**), indicating that the increase in Notch levels seen upon over-expression of $Amx^{\Delta ECD}$ and *Psn* knockdown is rather specific.

To obtain additional insights into why overexpression of $Amx^{\Delta ECD}$ inhibits Notch signaling whereas Amx^{FL} does not, we examined the expression and subcellular localization of the two proteins. We found that $Amx^{\Delta ECD}$ is expressed at significantly lower levels (~10%) compared to Amx^{FL} (**S7A and S7B Fig**), suggesting that the lack of phenotype induced by Amx^{FL} overexpression was not due to lower expression of this protein compared to $Amx^{\Delta ECD}$. Furthermore, we found that while Amx^{FL} exhibited a memebranous localization pattern when expressed in the developing wing disc (**S7C Fig**), $Amx^{\Delta ECD}$ was found in a more punctate pattern (**S7D Fig**). These differences in protein levels and localization may contribute to their different ability to modulate Notch signaling.

In summary, while over-expression of the full-length Amx protein did not cause any obvious defects, we serendipitously found that a truncated form of this protein that contains the small region that is highly conserved among all TM2D proteins can act as a potent inhibitor of Notch signaling when overexpressed in a several tissues including the wing disc, which is a tissue that endogenously expresses all three *TM2D* genes (**S7E Fig**). We also found through epistasis experiments that $Amx^{\Delta ECD}$ acts at the S3 cleavage step of Notch activation, suggesting that it likely regulates γ-secretase or factors/processes that facilitate this cleavage. This is further supported by our findings that overexpression of $Amx^{\Delta ECD}$ and knock-down of *Psn*, but not loss of *kuz*, both lead to accumulation of Notch both at the cell surface as well as intracellularly.

Null mutants of *TM2D* family genes have shortened lifespan

AD is an adult-onset age-dependent disease that worsens over time. While $TM2D3^{p.P155L}$ has been associated with LOAD [13] and $TM2D3^{p.P69L}$ has been recently reported in a proband with EOAD or frontotemporal dementia [22], there is no functional data that directly links this gene to an age-dependent neurological phenotype in any species. In *Drosophila*, knockdown of genes encoding subunits of the γ-secretase complex, *Psn* and *Nicastrin (Nct)*, specifically in adult neurons causes a shortening of lifespan phenotype which is accompanied by an age-dependent motor function decline [48]. Considering our results suggesting that Amx is involved in a process that relates to γ-secretase (**Fig 5**), we asked whether loss of *amx* causes an age-dependent phenotype in flies (**Fig 6**). To asssess the effect on lifespan, we compared the longevity of amx^{Δ} hemizygous male flies with control flies that also carry a genomic rescue construct (amx^{Δ} + *amx*) to neutralize the effect of genetic backgroud [13]. We selected males for our analysis because *amx* loss does not affect male fertility, allowing us to ignore any changes in lifespan that may be caused by alterations in fecundity [52]. In contrast to the rescued control animals that exhibit a median lifespan of 51 days, the median lifespan of *amx* null flies is significantly shorter at 27 days (**Fig 6A**, $p = 1.0x10^{-11}$). We next tested whether human *TM2D3* can substitute for the loss of *amx* in this context by introducing the humanized genomic rescue construct [13] into the *amx* null mutant background (amx^{Δ} + *hTM2D3*). These humanized *TM2D3* animals had a median lifespan of 33 days (**Fig 6A**). Although this effect seems to be statically significant ($p = 9.5x10^{-10}$) and suggests that human TM2D3 may have some activity in this context, we cannot rule out the possibility that other genetic factors may be contributing to this effect considering the weakness of the phenotypic rescue.

Next, considering that loss of *amx* is phenotypically indistinguishable from the loss of *amrt* and *bisc*, we assessed whether loss of *amrt* or *bisc* causes a similar lifespan shortening phenotype in adult flies. By comparing the lifespan of $amrt^{\Delta}$ or $bisc^{\Delta}$ to their respective genomic rescue controls, we found that both mutants are significantly short lived (**S8A–S8B Fig**). Median lifespan of $amrt^{\Delta}$ was 48 days compared to 63 days in rescued control flies ($p = 6.0x10^{-11}$), and median lifespan of $bisc^{\Delta}$ was 32 days compared to 48 days in rescued animals ($p = 3.0x10^{-12}$). The difference in the median lifespan of rescued animals for the three mutants could be due to differences in their genetic backgrounds. In summary, flies that lack *amx*, *amrt* or *bisc* are short lived, suggesting that *TM2D* genes contribute to maintaining a normal lifespan.

Amx is expressed in the adult brain and required in neurons to maintain a normal lifespan

To further study the role of *TM2D* genes in aging animals, we decided to perform additional experiments on *amx* null mutant flies, considering the link between its human ortholog to AD. Shortened lifespan seen in amx^{Δ} animals could be due to a number of reasons, including defects in the nervous system or other organs functionally affected by the loss of *amx*. Based on publicly available microarray [37], RNA sequencing (RNA-seq) [38] and single cell RNA-sequencing (scRNA-seq) [53] datasets, *amx* mRNA has been detected in the adult nervous system at low levels in a subset of neurons and glia cells (**S9 Fig**). To determine whether Amx protein can be detected in the adult nervous system, we generated an N'-tagged *amx* genomic rescue construct in which a 3xHA epitope is inserted immediately after the signal sequence of the Amx protein (**Fig 1A and 1B**), similar to the *UAS-3xHA*::*amx* transgene discussed earlier (**Fig 4A**). This tagged genomic rescue construct is able to rescue the female sterility and the maternal-effect neurogenic phenotype of amx^{Δ} (**Fig 1C and 1F**), indicating the epitope tag does not have a major effect on Amx function. Next, we verified expression of 3xHA::Amx in the female ovary through immunofluorescent staining and western blot (**S10 Fig**). Based on

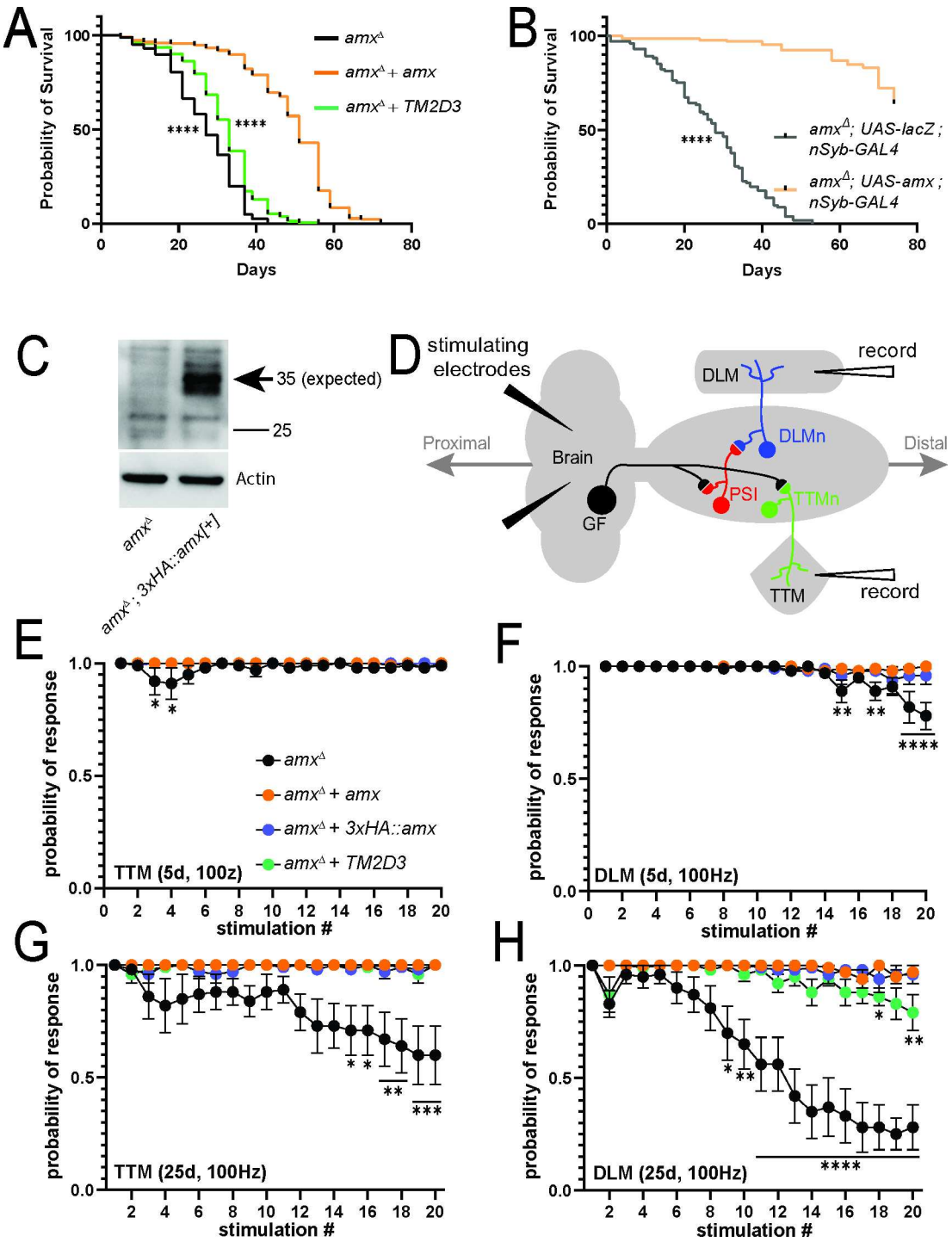

Fig 6. Loss of *amx* causes shortening of lifespan and age-dependent neurophysiological defects. (A) Lifespan assay shows amx^{Δ} animals (black, n = 247) have reduced lifespan compared to amx^{Δ} + *amx* controls (orange, n = 224). amx^{Δ} + human *TM2D3* flies (green, n = 234) have significantly longer lifespan than amx^{Δ} animals, but shorter than control. Animals were reared at 25˚C; Log-rank test (Mantel-Cox), **** = p<0.0001. (B) Restoring Amx expression specifically in neuronal cells rescues the reduced lifespan in *amx* null animals. LacZ overexpression was used as a control. Animals were reared at 25˚C; Log-rank test (Mantel-Cox), **** = p<0.0001. (C) Western blot of amx^{Δ}; *3xHA::amx* brains shows that 3xHA::Amx (predicted 35 kDa size) is expressed in the adult nervous system (arrow). Protein isolate from five brains was loaded per lane and Actin was probed as a loading control. (D) Schematization of the giant fiber electrophysiological recordings. Stimulating electrodes are inserted into the brain and recording electrodes record responses from the TTM and DLM muscles. (E-F) TTM muscles of 5d old amx^{Δ} mutants

(black) have a response similar to amx^{Δ} + *amx* controls (orange) while DLM muscles have small but significant decrease in response probability. *3xHA*::*amx* (blue) flies also perform as well as controls. (G-H) TTM and DLM response in 25d old amx^{Δ} mutants is significantly reduced. DLM response of 25d old amx^{Δ} + human *TM2D3* (green) flies is reduced compared to controls (I). Multiple unpaired t-tests with Holm-Šídák correction for multiple comparisons. * = $p<0.05$. ** = $p\leq0.01$. *** = $p<0.001$, **** = $p<0.0001$. Error bars show SEM. Additional data can be found in **S12–S14 Figs**.

https://doi.org/10.1371/journal.pgen.1009962.g006

immunostaining, we detected the highest signal of 3xHA::Amx in nurse cells of the ovary and observed that it localizes to the cell membrane as well as in intracellular puncta (**S10A and S10B Fig**). Based on western blot, we identified 3xHA::Amx at the predicted molecular weight [34.82 kDa (31.35 kDa for Amx, 3.47 kDa for the 3xHA tag)] (**S10C Fig**). Finally, we assessed the expression of 3xHA::Amx in the adult brain via immunostaining and western blot. While we did not observe a strong signal beyond background fluorescence based on immunofluorescence staining using an anti-HA antibody (**S11 Fig**), we detected 3xHA::Amx expression via western blot using brain extracts (**Fig 6C**). Therefore, in addition to *amx* mRNA that has been detected through multiple high-throughput transriptomic studies, Amx protein is also expressed in the adult brain, albeit at relatively low levels.

To determine a if *amx* is required neuronally, we reintroduced wild-type Amx specifically in neurons using *nSyb-GAL4* [54] in *amx* null animals. We found that the lifespan defect of amx^{Δ} can be significantly suppressed by this manipulation ($p<1.0x10^{-16}$, **Fig 6B**). In conclusion, Amx is expressed in the adult nervous system at relatively low levels, and required in neurons to maintain a normal lifespan.

amx null mutants show progressive motor and electrophysiological defects

Considering its neuronal requirement, we next tested whether loss of *amx* causes age-dependent behavioral defects. Since neuronal knockdown of γ-secretase genes in flies was reported to cause age-dependent climbing defects [48], we assessed whether *amx* null animals also show this phenotype. We found that amx^{Δ} mutants show a climbing defect as early as 5 days post-eclosion, which progresses in severity as time goes on (**S8C Fig**), suggesting that this gene is not only required to maintain normal lifespand but also for healthspan [55].

To directly assess whether *amx* is required for maintenance of neural function, we performed electrophysiology on amx^{Δ} animals and controls. The giant fiber system is a neuronal circuitry that is required for rapid escape responses in insects and has been used as a model circuitry to assess neuronal function in a quantitative manner in adult flies [56]. This pathway can be activated through direct stimulation of the brain and outputs of the circuit can be monitored by recording the responses from tergotrochanteral (TTM) and dorsal longitudinal (DLM) muscles (**Fig 6D**). For a given time point, we applied multiple stimulations at different frequencies (20, 50, and 100 Hz; **Figs 6E–6H** and **S12–S14**), and measured how well these muscles respond to each stimulation. Healthy neurons can follow the stimulations showing a 'probability of response' that is close to 1.0, but neurons that are unhealthy show decreased probability of response, which indicates failure of the signal to travel from the brain to the muscles [57,58].

At 5 days post-eclosion, amx^{Δ} flies have a minor but significant failure rate at later stimulations at 100 Hz in the DLM muscle compared to control animals (rescued with a wild-type *amx* [amx^{Δ} + *amx*] or N'-3xHA tagged *amx* [amx^{Δ} + *3xHA*::*amx*]; **Fig 6F**). Additionally, amx^{Δ} animals show only slight, early stimulation failure rates in the TTM at 50 and 100 Hz at 5 days (**Figs 6E and S12D**). At 15 days post-eclosion, amx^{Δ} animals still only show mild failure rate in the TTM at 100 Hz (**S13E Fig**) but begin to show a significant increase in failure rate compared to control animal recordings from the DLM at 50 and 100 Hz (**S13D and S13F Fig**). At 25 days post-eclosion, the defects in the DLM increase in severity for 50 and 100 Hz compared to

rescued controls (**Figs 6H and S14D**). At this time point, the TTM also begins to show a significant failure rate in amx^{Δ} animals at 100Hz compared to rescued animals but not at lower frequencies (**Figs 6G, S14A and S14C**). Interestingly, unlike in the lifespan assay in which the human *TM2D3* did not dramatically suppress the amx^{Δ} mutant phenotype (**Fig 6A**) and in the fertility/neurogenesis assay in which the human TM2D3 showed ~50% activity of the fly Amx protein (**Fig 1C**), we found that human TM2D3 is able to significantly suppress the electrophysiological defects close to the level of fly Amx (**Figs 6E–6H and S12–S14**). In summary, loss of *amx* causes an age-dependent decline in neuronal function, and this defect can be fully rescued by both fly and human *TM2D3*, indicating an evolutionarily conserved role of this gene in healthy aging.

Discussion

In this study, we functionally characterized *TM2D* genes through gene knockout and over-expression strategies in *Drosophila melanogaster* to gain biological knowledge on this understudied but evolutionarily conserved gene family that has been implicated in AD. We first showed that the knockout allele of *amx* (*Drosophila* homolog of *TM2D3*) generated by CRISPR is phenotypically indistingusiable from the classic amx^{1} allele and displays female sterility and a maternal-effect neurogenic defect. Recently, we reported that this allele also shows a maternal-effect inductive signaling defect to specify the mesoectoderm during embryogenesis which is another Notch-dependent event [59], demonstrating that *amx* is maternally required for multiple Notch signaling dependent processes during embryogenesis. In addition, we generated the first knockout alleles of *amrt* (*Drosophila* ortholog of *TM2D2*) and *bisc* (*Drosophila* ortholog of *TM2D1*) and documented that each null allele phenotypically mimics the loss of *amx*. Furthermore, we revealed that the triple knockout of all three *TM2D* genes in *Drosophila* show identical maternal-effect neurogenic phenotypes without exhibiting other obvious Notch signaling-related developmental defects. Moreover, although the over-expression of the full-length Amx do not cause any scorable defects, we serendipitously found that expression of a truncated form of Amx that lacks the majority of the extracellular domain can strongly inhibit Notch signaling in the developing wing imaginal disc, a tissue in which all three fly *TM2D* genes are expressed endogenously. Through genetic epistatic experiments using newly generated *UAS-Notch* transgenic lines, we mapped this inhibitory effect to the γ-secretase cleavage step of Notch activation. Subsequently, we found that *amx* null animals have a shortened lifespan, a phenotype that can be rescued by reintroduction of Amx in neurons. This shortening of lifespan phenotype was also seen in *amrt* and *bisc* null flies, suggesting that these three genes may also function together in the aging brain. Finally, through assement of climibing behavior and electrophysiological recordings of the giant fiber system, we showed that *amx* null flies show age-dependent decline in neural function. In summary, we demonstrate that all three *TM2D* genes play critical roles in embryonic Notch signaling to inhibit the epithelial-to-neuron cell fate transformation as maternal-effect genes, and that *amx* is required for neuronal maintenance in the adult nervous system, a function that may be related to the role of human *TM2D3* in AD.

Within commonly used genetic model organisms, *TM2D* genes are found in multicellular animals (both in invertebrates and in vertebrates) but are absent in yeasts (e.g. *Saccharomyces cerevisiae*, *Schizosaccharomyces pombe*) and plants (e.g. *Arabidopsis thaliana*), suggesting that this family of genes arose early in the metazoan lineage. In humans and flies, there are three *TM2 domain-containing* genes (*TM2D1*, *TM2D2*, *TM2D3* in *Homo sapiens*; *bisc*, *amrt*, *amx* in *Drosophila melanogaster*, respectively), each corresponding to a single gene in the other species. Interestingly, this 1:1 ortholog relationship is also seen in mouse (*Tm2d1*, *Tm2d2*,

Tm2d3), frog (*Xenopus tropicalis*: *tm2d1*, *tmd2d*, *tm2d3*) zebrafish (*Danio rerio*: *tm2d1*, *tm2d2*, *tm2d3*) and worm (*Caenorhabditis elegans*: *Y66D12A.21*, *C02F5.13*, *C41D11.9*) (**S1 Fig**). In general, most genes have more paralogous genes in humans compared to flies (for example, one *Drosophila Notch* gene corresponding to four *NOTCH* genes in human) as vertebrates underwent two rounds of whole-genome duplication (WGD) events during evolution [60]. Furthermore, teleosts including zebrafish underwent an extra round of WGD [61], leading to formation of extra duplicates in 25% of all genes (e.g. one *NOTCH1* gene in human corresponds to *notch1a* and *notch1b* in zebrafish). Hence it is interesting that each of the three *TM2D* genes remained as single copy genes in various species despite whole genome level evolutional changes, suggesting that there may have been some selective pressure to keep the dosage of these genes consistent and balanced during evolution.

Although the *in vivo* functions of *TM2D1* and *TM2D2* have not been studied extensively in any organism, several lines of studies performed in cultured cells suggest that these genes may also play a role in AD pathogenesis. Through an yeast-two hybrid screen to identify proteins that bind to Aβ42, Kajkowski et al. identified TM2D1 and referred to this protein as BBP (beta-amyloid binding protein) in their study [24]. They further showed that TM2D1 can also interact with Aβ40, a non-amyloidogenic form of Aβ, and mentioned that they have preliminary data that it also binds to APP (Kajkowski et al., 2001). The interaction between Aβ peptides and TM2D1 was shown to require the extracellular domain as well as a portion of the first transmembrane domain of TM2D1. Because overexpression of TM2D1 in a human neuroblastoma cell line (SH-SY5Y) increased the sensitivity of these cells to cell death caused by incubation with aggregated Aβ and since the DRF motif was found to be required for this activity, the authors of this original study proposed that TM2D1 may function as a transmembrane receptor that mediates Aβ-toxicity [24]. However, a follow-up study from another group refuted this hypothesis by providing data that TM2D1 is not coupled to G proteins using a heterologous expression system in *Xenopus* oocytes [62]. Therefore, although the physical link between TM2D1 and Aβ42 is intriguing, the significance of this interaction and its role in AD pathogenesis has been obscure.

To our surprise, loss of *bisc/TM2D1* and *amrt/TM2D2* were phenotypically indistinguishable from the loss of *amx/TM2D3* in *Drosophila*. The zygotic loss of each gene did not exhibit any strong developmental defects into adulthood, despite their relatively ubiquitous expression pattern according to large transcriptome datasets [37,38]. Furthermore, the loss of either *amrt* or *bisc* caused a reduction of lifespan, again mimicking the loss of *amx*. More interestingly, the triple null mutants are viable and do not exhibit any morphological defect, suggesting that these genes are not required zygotically during development. In contrast, maternal loss of any single *TM2D* gene causes a strong embryonic neurogenic defect, which is also seen in embryos laid by triple knockout animals. Neurogenic defect is a classical phenotype in *Drosophila* that was originally reported in the mid-1930s [63,64], and the study of mutants that show this phenotype led to the establishment of the core Notch signaling pathway in the late 1980's and early 1990's [7,65]. Although the study of neurogenic phenotypes and genes has a long history, this phenotype is a very rare defect that has so far been associated with only 19 genes according to FlyBase [66], prior to this work. Seven genes show this defect as zygotic mutants [*aqz*, *bib*, *Dl*, *E(spl)m8-HLH*, *mam*, *N* and *neur*], seven genes are zygotically-required essential genes with large maternal contributions (hence the need to generate maternal-zygotic mutants by generating germline clones to reveal the embryonic neurogenic defect) [*Gmd*, *Gmer*, *gro*, *Nct*, *O-fut1*, *Psn* and *Su(H)*], one gene has only been investigated by RNAi (*Par-1*) and four genes including *amx* are non-essential genes that show maternal-effect neurogenic defects (*amx*, *brn*, *egh*, *pcx*). Hence, our study has revealed two new genes that are evolutionarily closely linked to *amx* in this Notch signaling related process.

The similarity of sequences and phenotypes caused by loss of *amx*, *amrt* and *bisc* suggests that the proteins encoded by these genes may function together. The lack of additive or synergistic phenotypes in the double and triple null mutant flies also support this idea. Interestingly, high-throughput proteomics experiments based on co-immunoprecipitation mass spectrometry (co-IP/MS) from human cells have detected physical interactions between TM2D1-TM2D3 [67] and TM2D2-TM2D3 [68], suggesting these proteins may form a protein complex. Further biochemical studies will be required to clarify the functional relationship between the three TM2D proteins. Two additional mammalian datasets further support our hypothesis that these three proteins functions together. First, all three *TM2D* genes were identified through a large scale cell-based CRISPR-based screen to identify novel regulators of phagocytosis [69]. Individual knockout of *TM2D* genes in a myeloid cell line was sufficient to cause a similar phagocytic defect based on the parameters the authors screened for (e.g. substrate size, materials to be engulfed). Although the authors of this study did not generate double or triple knockout cell lines to determine whether there were any additive or synergistic effects when multiple *TM2D* genes were knocked out, this suggests that these three genes may function together in phagocytosis. The authors further note that because these genes are broadly expressed in diverse cell types beyond phagocytic cells in the nervous system [70], they may play other roles in the brain, consisnet with our finding that *amx* is required neuronally to maintain a normal lifespan. It would be interesting to explore whether age-dependent phenotypes seen in *TM2D* null mutants can also be suppressed through glial specific rescue experiments to understand the *in vivo* significance of this group's *in vitro* findings. Second, preliminary phenotypic data from the International Mouse Phenotyping Consortium [71] indicates that single knockout of mice of *Tm2d1* (https://www.mousephenotype.org/data/genes/MGI:2137022), *Tm2d2* (https://www.mousephenotype.org/data/genes/MGI:1916992) and *Tm2d3* (https://www.mousephenotype.org/data/genes/MGI:1915884) are all recessive embryonic lethal prior to E18.5. Although detailed characterization of these mice will be required and further generation of a triple knockout line is desired, the shared embryonic lethality may indicate that these three genes potentially function together in an essential developmental paradigm during embryogenesis in mice.

Our attempts to unravel the function of Amx through overexpression of the full-length protein was uninformative since this manipulation did not cause any scorable phenotype. However, we serendipitously found that a truncated form of Amx, which only contains the most conserved region of TM2D family proteins, has the capacity to strongly inhibit Notch signaling during wing and notum development. These results were surprising because we did not see any wing or bristle defects in the triple *TM2D* gene family knockout flies, even though all three genes are endogenously expressed in the wing imaginal disc. Through epistasis experiments using a set of new *UAS-Notch* transgenic lines, we found $Amx^{\Delta ECD}$ to inhibit Notch signaling at the S3 cleavage step which is mediated by the γ-secretase complex. This data is consistent with earlier epistasis experiments performed on amx^{1} in the context of embryonic neurogenesis [25], further supporting the idea that *amx* may regulate γ-secretase function *in vivo*. We further determined that over-expression of $Amx^{\Delta ECD}$ in the wing imaginal disc causes an accumulation of Notch protein within the cell and at the cell membrane. This phenotype is similar to what is seen upon knockdown of *Psn* in the wing imaginal disc, which is consistent with earlier findings showing Notch accumulation at the cell membrane in neuroblasts of *Psn* mutants [72]. In summary, we showed that ectopic over-expression of a portion of Amx that is conserved among all TM2D proteins causes a strong Notch signaling defect by disrupting a process that realtes to γ-secretase, providing additional links between Amx/TM2D3 and AD.

By aging the *amx* null male flies that are visibly indistinguishable from the control flies (*amx* null flies with genomic rescue constructs), we found that loss of *amx* causes a significant

decrease in lifespan, a phenotype that we observed in *amrt* and *bisc* null flies. By generating a functional genomic rescue transgene in which Amx is tagged with an epitope tag, we found that this protein is expressed in the adult brain. The short lifespan defect of *amx* null flies was effectively rescued by reintroduction of Amx in neurons, demostrating the importance of this gene in this cell type. In addition to the lifespan defect, *amx* null flies also exhibited an age-dependent climing defect, suggesting that their neural function declines with age. By further performing electrophysiological recordings of the giant fiber system, which is a model circuit that is frequently used in neurological and neurodegenerative research in *Drosophila* [56,73–75], we found that there is indeed an age-dependent decline in the integrity of this circuit. Through this assay, we observed that the DLM branch of the giant fiber system begins to show failures earlier than the TTM branch. The DLM is activated by giant fiber neurons that chemically synapse onto PSI (peripherally synapsing interneuron) neurons through cholinergic synapses, which in turn chemically synapse onto motor neurons (DLMn which are glutamatergic) through cholinergic connections. The TTM, in contrast, is activated by giant fiber neurons that electrically synapse onto motor neurons (TTMn which are glutamatergic) through gap junctions, causing a more rapid response. Considering the difference in the sensitivity of the two branches, cholinergic neurons/synapses may be more sensitive to the loss of *amx*, a neuronal/synaptic subtype that is severely affected in AD in an age-dependent manner [76].

How does *amx* maintain neuronal function in aged animals and is this molecular function related to AD? One potential molecular mechanism is through the regulation of γ-secretase in the adult brain. By knocking down subunits of the γ-secretase complex, *Psn* and *Nct*, specifically in adult neurons, Kang et al. showed that reduction of γ-secretase function decreases lifespan, which was associated with climbing defects as well as histological signs of neurodegeneration [48]. The requirement of γ-secretase components in neuronal integrity has also been reported in mice [77–81], suggesting this is an evolutionarily conserved phenomenon. Interestingly, the role of the γ-secretase complex in neuronal maintenance is unlikely to be due to defects in Notch signaling because neurodegeneration has not been observed upon conditional removal of Notch activity in post-developmental brains in flies and in mice [82]. While the precise function of γ-secretase in neuronal maintenance is still unknown, several possibilities including its role in regulating mitochondrial morphology [80] and calcium homeostasis [83,84] has been proposed based on studies in *C. elegans* and mice. Investigating whether Amx does indeed regulate γ-secretase in adult neurons and whether it impacts the aforementioned processes will likely facilitate our understanding on how this gene regulates neuronal health. Furthermore, considering that *TM2D3* and other *TM2D* genes have been proposed to function in phagocytic cells, and because phagocytosis process plays many roles beyond engulfment of toxic Aβ molecules in the nervous system [85], Amx may also be playing a role in engulfing unwanted materials that are harmful for the adult brain. For example, loss of the phagocytic receptor Draper in glia cells causes age-dependent neurodegeneration that is accompanied by accumulation of non-engulfed apoptotic neurons throughout the fly brain [86]. Interestingly, a recent study has shown that over-expression of phagocytic receptors can also promote neurodegeneration [87], indicating the level of phagocytic activity needs to be tightly controlled *in vivo*. Further studies of amx^{Δ} mutants (as well as amx^{Δ} $amrt^{\Delta}$; $bisc^{\Delta}$ triple mutants) in the context of phagocytosis will likely reveal the precise molecular function of Amx and other TM2D proteins in this process.

Finally, could there be any molecular link between the role of *TM2D* genes in Notch signaling (proposed based on experiments in *Drosophila*) and phagocytosis (revealed based on mammalian cell culture based studies), or are they two independent molecular functions of the same proteins? All TM2D proteins have two transmembrane domains connected by a short intracellular loop, making them an integral membrane protein. By tagging the *amx* genomic

rescue construct with a 3xHA tag that does not influence the function of Amx, we observed that 3xHA::Amx is localized to the plasma membrane as well as intracellular puncta, which likely reflects intracellular vesicles. Interestingly in embryos laid by amx^{Δ} mutant females, we observed a mild and transient but significant alteration in Notch distribution during early embryogenesis [59]. Moreover, we observed a strong accumulation of Notch when we overexpressed $Amx^{\Delta ECD}$ in the developing wing primordium. These data indicate that Amx may affect protein trafficking, which in turn may impact the processing of Notch by the γ-secretase complex. Indeed, Notch signaling is highly regulated by vesicle trafficking and alterations in exocytosis, endocytosis, recycling and degradation all impact the signaling outcome [88,89]. In fact, multiple studies have proposed that γ-secretase cleavage occurs most effectively in acidified endocytic vesicles [90,91]. Hence, while *amx* may be specifically required for the proper assembly or function of the γ-secretase complex, it may alternatively be necessary to bring Notch and other substrates to the proper subcellular location for proteolytic cleavages to occur efficiently. The subcellular localization differences observed between the punctate $Amx^{\Delta ECD}$, which causes a dramatic Notch signaling defect accompanied by mistrafficking of Notch, and the membranous Amx^{FL}, which does not have this effect, may further support the idea that Amx function as a trafficking module. Similar to Notch signaling, phagocytosis also requires coordination of many cellular trafficking events to expand the plasma membrane to form a phagophore, internalize the particle of interest to generate a phagosome, and fuse the phagosome to lysosomes to degrade its content [92]. By studying the role of *TM2D* genes and proteins in embryonic Notch signaling, phagocytosis and age-dependent neuronal maintenance, we will likely understand the precise molecular and cellular function of this evolutionarily conserved understudied protein family, which will likely lead to further understanding of molecular pathogenesis of AD and other human diseases. Considering the phenotypic similarities of *amrt* and *bisc* to *amx* in *Drosophila* embryonic neurogenesis, the similarities between *TM2D1-3* in human cells in the context of phagocytosis, and the similarities of *Tm2d1-3* knockout mice in the context of embryogenesis, we propose that studies of rare genetic variants, epigenetic regulators or proteomic changes in other *TM2D* genes may reveal novel risk factors or biomarkers in epidemiologic study of AD and other forms of dementia.

Materials and methods

Protein alignment and phylogenetic analysis of TM2D family genes

For informatic analysis, we downloaded the FASTA files corresponding to the following proteins from Uniprot (https://www.uniprot.org/). Human (*Homo sapiens*) TM2D1 (Q9BX74), TM2D2 (Q9BX73), TM2D3 (Q9BRN9); Mouse (*Mus musculus*) Tm2d1 (Q99MB3), Tm2d2 (Q8R0I4), Tm2d3 (Q8BJ83); Frog (*Xenopus tropicalis*) tm2d1 (A0A6I8QKF8), tm2d2 (Q5M8E3), tm2d3 (Q07FZ2); Zebrafish (*Danio rerio*) tm2d1 (A5PLH4), tm2d2 (Q6DHN3), tm2d3 (A5PLF5); Fly (*Drosophila melanogaster*) CG10795 (Q9W2H1), CG11103 (Q9VY86), amx (Q9U4H5); Worm (Caenorhabditis elegans) Y66D12A.21 (Q95PJ8), C02F5.13 (P61228), C41D11.9 (Q95QZ5). Protein alignment was performed using Clustal Omega using default parameters (http://www.clustal.org/omega/). Phylogenetic analysis was performed using MAFFT (multiple alignment using fast Fourier transform) version 7 (https://mafft.cbrc.jp/alignment/server/) through UPGMA (unweighted pair group method with arithmetic mean) and Neighbor-Joining methods using default parameters.

Drosophila strains and fly husbandry

Drosophila melanogaster stocks used in this study are listed in **S1 Table**. Some strains were generated in house for this study (see below), and others were obtained from Bloomington

Drosophila Stock Center (BDSC) and other sources. Flies were kept on standard media and maintained at room temperature (21–23˚C). Crosses were performed at 25˚C in an incubator unless otherwise stated. Genotypes of the flies shown in each figure panel are listed in **S2 Table**.

Generation of *amx* overexpression transgenes

To generate the untagged *UAS-amx* transgene, we PCR amplified the open reading frame (ORF) of *amx* derived from the cDNA clone GH02974 (Genbank ID: AF181623, *Drosophila* Genomics Resource Center, Indiana University) with NotI and XbaI restriction sites on the 5' and 3' end, respectively, and subcloned this fragment into pUASTattB [93]. The cDNA templates used to generate the UAS constructs to overexpress 3xHA epitope tagged full-length (*UAS-3xHA*::amx^{FL}) and truncated (*UAS-3xHA*::$amx^{\Delta ECD}$) Amx were synthesized by Genewiz. The *amx* ORF used for these constructs is identical to the GH02974 clone, which is also identical to the coding sequence of the genomic rescue construct we reported in [13]. A 3xHA epitope sequence (N'-YPYDVPDYAGYPYDVPDYAGSYPYDVPDYA-C') was inserted after the signal sequence (SS) as predicted by SignalP 4.1 (http://www.cbs.dtu.dk/services/SignalP-4.1) and Phobius (http://phobius.sbc.su.se). A 968 bp fragment corresponding to 3xHA tagged full-length Amx was synthesized with NotI and XbaI restriction sites on the 5' and 3' end respectively. Furthermore, a 464 bp fragment corresponding to 3xHA::$Amx^{\Delta ECD}$ was designed based on the full-length 3xHA::Amx construct, but with the majority of the endogenous Amx N'-end removed leaving the SS, epitope tag, and TM2 domains intact. We subcloned the synthesized fragments into pUASTattB [93] via restriction enzyme cloning utilizing the NotI and XbaI cut sites. We then injected the final plasmids into VK37 (*PBac{y[+]-attP}VK00037*) attP docking site [43] and injected animals were crossed to *y w* and screened for the presence of the $white^{+}$ marker encoded in the pUASTattB backbone in a $white^{-}$ background. Positive animals were then crossed to *SM6a* to create a balanced stock. One line for each transgenic construct was chosen for this study.

Generation of a N'-tagged *amx* genomic rescue transgene

The *3xHA*::*amx* genomic rescue transgene was designed and constructed based on the non-tagged genomic rescue construct we reported in [13]. A ~3.3kb region including the full *amx* gene has the ability to fully rescue the maternal effect neurogenic phenotype of amx^{1} [13] and amx^{Δ} (this study). We inserted a 3xHA sequence into the pattB-amx genomic rescue construct described in [13] via NEBuilder HiFi DNA Assembly. 3xHA was inserted after the predicted signal sequence (N'-ATMRLQRQCIVVNMRSAIVLIMIFVLTGIRNSET-C') to tag Amx at its N'. pUASTattB-3xHA::amx^{FL} described above was used as a template to amplify and add appropriate homology arms to the SS-3xHA::Amx DNA sequence with the primers 5'-CCCC GCTCTATCTGACCAAAGCCACCATGAGGCTCCAACGAC-3' and 5'-AAAACTAAACT AAGAACGGACTACTATATGTAAAGTGAGCCATCCGC-3' using Q5 High-Fidelity 2X Master Mix (M0492S, NEB). These and other Oligo DNA were synthesized by Sigma Aldrich. The section of pattB-amx plasmid containing the *amx* regulatory elements was linearized by PCR using Q5 polymerase and primers 5'-CGTTGGAGCCTCATGGTGGCTTTGGTCAG ATAGAGCG-3' and 5'-GCTCACTTTACATATAGTAGTCCGTTCTTAGTTTAGTTTTA CAGGGGT-3', which add appropriate homology arms to allow for assembly with the 3xHA::Amx fragment. The construct was assembled following the protocol described by NEBuilder HiFi DNA Assembly Master Mix (NEB Catalog #E2621S) and confirmed by Sanger sequencing. The validated construct was injected into embryos expressing ϕC31 integrase with a 2nd chromosome *attP* docking site (VK37) [43]. We also injected a empty pattB plasmid into the same docking site to generate a control like (*pattB[w+]*). Transgenic flies were isolated based on eye color (w^{+} encoded by the *mini-white* gene in pattB vector) and balanced over *SM6a*.

Generation of the *amrt*$^{\Delta}$ mutant

The *amrt (CG11103)* null allele was created based on a method we described in [33]. We selected gRNA (guide RNA) target sites using CRISPR Optimal Target Finder (http://targetfinder.flycrispr.neuro.brown.edu/). sgRNAs (single gRNA) expressing plasmid was generated using the pCFD3-dU6:3 gRNA vector (Plasmid ID: #49410, Addgene) as described in [94]. Oligo DNA to generate the upstream sgRNA plasmid were 5'-GTCGCGCTGCGTGCCTGTATCGCT-3' and 5'-AAACAGCGATACAGGCACGCAGCG-3'. Oligo DNA to generate the downstream sgRNA plasmid were 5'-GTCGTCCTCGGGCAGCAAATTGT-C' and 5'-AAACACAATTTGCTGCCCGAGGA-3'. Donor plasmid containing the *yellow*$^{body+}$ marker (y^{body+}) to be integrated into the *amrt* locus via HDR was generated through NEBuilder HiFi DNA Assembly. Primers amplifying and adding homology arms to a pBH vector [95] backbone were 5'-GATGCTGTTAGACTAACGGTGTATATCTAGAGCCGTCCCGTCAAG-3' and 5'-CCGCAAGCAATGGCCAAACTGGGTCCTCGAGTCGACGTTG-3'. Primers for amplifying the *ybody*$^{+}$ insert and adding homology arms from P{ybody+} plasmid [33] were 5'-CAGACAACACGATGCCCAAGCGGATCGCTTGATGTTGTTTTGTTTTG-3' and 5'-TGCCGTCCTCGGGCAGCAAATGGAAGGAACCTGCAGGTCAACG-3'. All plasmids were verified by Sanger sequencing. *y*, *w*, *iso#6(X); attP2{nos-Cas9}* [33] embryos were injected with 25 ng/ul concentration of each sgRNA plasmid mixed with 150 ng/ul of the y^{body+} donor plasmid. Resulting adults were crossed to *y w* animals and offspring screened for the presence of the y^{body+} marker (dark body color instead of yellow body). Positive animals were crossed to the *FM7c* balancer to establish the lines and were molecularly genotyped (see below).

Generation of the *bisc*$^{\Delta}$ mutant

The *bisc* (*CG10795*) null allele was generated using the same strategy discussed above that was used to generate the *amrt* null allele. Oligo DNAs to generate the upstream sgRNA plasmid were 5'-GTCGTATGAGGGACCATGTACAT-3' and 5'-AAACATGTACATGGTCCCTCATA-3'. Oligo DNA to generate the downstream sgRNA plasmid were 5'-GTCGAGGCGGTGGTGGTGTTCTGT-3' and 5'-AAACACAGAACACCACCACCGCCT-3'. Primers amplifying and adding homology arms to a pBH vector backbone were 5'-GTAGACACACGGCATAGATGGTATATCTAGAGCCGTCCCGTC-3' and 5'-GAAGAAGTTGACAATGTGTTGGGTCCTCGAGTCGACGTTG-3'. Primers for amplifying the *ybody*$^{+}$ insert and adding homology arms from p{ybody+} plasmid were

5'-AATTGTATGAGGGACCATGTAGGATCGCTTGATGTTGTTTTG-3' and 5'-GTTGACCTGCAGGTTCCTGTTGGCGGGAGCTCTTTCTC-3'. All plasmids were verified by Sanger sequencing. *y*, *w; iso#2(2); attP2{nos-Cas9}* embryos were injected with 25 ng/ul concentration of each sgRNA plasmid mixed with 150 ng/ul of the y^{body+} donor plasmid. Resulting adults were crossed to *y*, *w* animals and offspring screened for the presence of the y^{body+} marker. Positive animals were crossed to the *SM6a* balancer to establish the lines and were molecularly genotyped (see below).

Detection of *TM2D* mRNA expression through RT-PCR

The presence or absence of mRNA corresponding to *TM2D* genes were determined using RT-PCR (Reverse Transcription-Polymerase Chain Reaction). Whole body RNA was isolated from adult animals through standard TRIzol/chloroform RNA extraction protocol. We prepared cDNA with iScript Reverse Transcription Supermix, (#1708840, BioRad). PCR was done using Q5 polymerase (M0492S, NEB). Primers used to detect the presence of *amx* cDNA were 5'-TCCCCGCTCTATCTGACCAA-3' and 5'-GCTCTGTTGCCACATTTCCG-3'. Primers to detect the presence of *amrt* cDNA were 5'-CTACGGACTACTGGCGTTCC-3' and 5'-CCCG

TTTGACCGAGACAGAA-3'. Primers to detect the presence of *bisc* cDNA were 5'-CCCCGC GAACTGCAATAAAC-3' and 5'-CACAACCTGCAGGGCTATCA-3'. Primers targeting *TM2D* cDNA were annealed at 68^0 C, extended for 30s at 72^0 C for 30 cycles. Primers for control gene *rp49* were 5'-TCTGCATGAGCAGGACCTC-3' and 5'-CGGTTACGGATCGAACAAG-3' [96]; annealed at 64^0 C and extended 30s for 30 cycles. The same protocol was used to assess the mRNA expression of *TM2D* genes in wing imaginal discs.

Generation of an *amrt* genomic rescue construct

Genomic DNA was isolated from *y*, *w*, *iso#6; +/+; attP2{nos-Cas9}* animals using PureLink Genomic DNA Mini Kit (Cat no. K1820-01, Invitrogen). Genomic region fully containing the *amrt* (*CG11103*) locus and neighboring sequences was amplified by PCR using the primers 5'-TATATACTCGAGcgcgaaactttcgatttcc-3' and 5'-TATATAGAATTCatcgaatgtagagatgggc-3' (small letters indicate annealing region) which added EcoRI and XhoI restriction sites for follow-up cloning into the pattB vector [93]. The pattB-amrt plasmid was injected into VK37 [43] docking site on the second chromosome. Eclosed animals were crossed to *y*, *w* and screened for the w^+ marker in the subsequent generation. Positive animals were then crossed to *SM6a* to create a balanced stock.

Generation of *biscotti*::*GFP* fosmid transgenic line

A ~40kb genomic fosmid construct in which *bisc* is C'-tagged with GFP and other epitopes [36] (*bisc*::*GFP*, FlyFos021003, *Drosophila* TransgeneOme Resource ID: CBGtg9060C1139D) was obtained from Source BioScience. Bacterial colonies were provided to GenetiVision Corp. for DNA preparation, injection into VK33 (*PBac{y[+]-attP}VK00033*) on the third chromosome [43], selection, and balancing of fly lines using the *TM3*, *Sb* balancer. Three independent lines were generated and all three behaved in a similar manner. One line was chosen for the experiments performed in this study.

Creation of Notch overexpression transgenic lines

All transgenic constructs were generated by Gateway (Thermo Fisher Scientific) cloning into the pUASg-HA.attB plasmid [93]. First, we generated Gateway compatible plasmid that contains the full-length Notch open reading frame. We subcloned the full-length *Notch* (N^{FL}) open reading frame into the pDONR223 plasmid based on a cDNA clone provided by Dr. Spyros Artavanis-Tsakonas [97], which was mediated by a Gateway reaction using BP clonase II (Thermo Fisher Scientific, #11789100) following a PCR reaction and addition of attB sites to the amplicon [98,99]. Truncated *Notch* constructs were generated by Q5 site-directed mutagenesis (NEB) with the following primers:

N^{EXT}: 5'-GCGGCCAAACATCAGCTG-3' and 5'-GTGCATTTTGTTAATCCAAAAACAA ATCC-3'.

N^{ICD}: 5'-GTCTTGAGTACGCAAAGAAAG-3' and 5'-CATGGTGAAGCCTGCTTT-3'.

$N^{\Delta EGF1\text{-}18.LNR}$ (two-step mutagenesis): 5'-CTGAGCGATGTGGACGAGTGCGCATCGA AT-3' and 5'-CAACGCGGTATCAGTTCC-3' followed by mutagenesis with 5'-AACAAGA CCCAGTCACCG-3' and 5'-CATGGCACGTTGTTGCTC-3'.

All constructs were fully sequenced (Sanger), and cloned into pUASg-HA.attB via LR clonase II (Thermo Fisher Scientific, #11791020). All expression constructs were inserted into VK37 integration site [43]. Two transgenic lines were established for each and one line each was used for this study.

Embryo collection, staining and imaging

Embryo collection, staining and imaging was performed as previously described [13]. In brief, virgin females that are homozygous for each or all *TM2D* gene mutations, with or without genomic rescue constructs, were crossed to males flies of the same genotype or *Canton-S* males, and allowed to mate in a vial for 24 hrs. Flies were then transferred to a bottle with a grape juice plate supplemented with active yeast and allowed to lay eggs overnight. Embryos were then gently collected using a paint brush and their chorions were removed by 1.5 minute incubation in 66% bleach. Dechorionated embryos were then washed with water and fixed in 4% paraformaldehyde/PBS(phosphate buffered saline)/n-heptane solution for 30 minutes at room temperature. Fixed embryos were washed and stored in 100% methanol at -20˚C until use. Fixed embryos were rehydrated and rinsed with 0.03% Triton-X in PBS (PBST). A primary antibody to label neuronal nuclei [anti-Elav, rat monoclonal (7E8A10) [100], 1:200, Developmental Studies Hybridoma Bank (DSHB)] was applied in a solution of PBST/5% normal donkey serum (NDS)/0.1% NaN_3 overnight at 4˚C. Embryos were further washed with PBST upon removal of the primary antibody, and a secondary antibody (donkey anti-rat-Alexa488, 1:500; Jackson ImmunoResearch #712-545-153) was applied for 1 hour at room temperature. Stained embryos were washed in PBST and mounted onto glass slides using Vectashield with DAPI (4',6-diamidino-2-phenylindole, Vector labs). Embryos were imaged using Ti2E Spinning Disc confocal microscope (Nikon) and images analyzed using NIS software (Nikon).

Egg hatching assay

Egg hatching assay was performed as previously described [13]. Embryos were collected and dechorionated as described above. Dechorionated embryos were suspended in PBS and placed in 12-well cell culture dishes. The dishes were then placed in a 25˚C incubator for 24 hours. The ratio of hatched to unhatched embryos after the 24 hour period was recorded for each genotype and used to calculate hatching rate (%). This was repeated at least 3 times and statistical analysis and graph generation was performed using GraphPad Prism 9.0 software. We performed one-way ANOVA followed by Dunnett test or t-test. **** = p-value $\leq$0.0001.

Imaging of adult flies

Heads and wings from adult flies were removed from the body using fine dissection scissors and imaged directly using a MZ16 microscope (Leica) with attached Microfire camera (Optronics) using ImagePro Plus 5.0 acquisition software (Media Cybernetics). Extended focus function was used to obtain deep focus images out of Z-stack images. Imaging of the dorsal thoraxes (nota) were described in [101] with slight modifications. In brief, legs, head, and abdomen were removed from thoraxes with fine dissection scissors. Then, the dissected thoraxes were then placed in 10% KOH at 95˚C. for 10 min to dissolve soft tissue. Thoraxes were then further trimmed with scissors prior to imaging and mounted on a glass slide with spacers using 75% glycerol/25% ethanol solution. Photos were taken using microscope system and imaging software as above.

Immunostaining and imaging of *Drosophila* wing imaginal discs, ovaries or brains

Wing discs from wandering larvae or ovaries and brain from adult flies were dissected in 1x PBS and fixed for 30 minutes in 4% paraformaldehyde in PBS. Tissues were then washed with 0.2% PBST for total Notch staining or with cell-culture grade PBS (Thermo Fisher Scientific,

#10010023) for extracellular Notch staining. All antibodies used in this study are listed in **S1 Table**. Primary antibodies [mouse anti-Notch intracellular domain (NICD) (1:50; DSHB, C17.9C6), mouse anti-Cut (1:100; DSHB, 2B10), rat anti-HA (1:100, Sigma-Aldrich, 11867423001), or mouse anti-NECD (1:100; DSHB, C458.2H)] were applied in 0.2% PBST or PBS with 5% NDS/0.1% NaN_3 overnight at 4˚C. Tissue was then washed with 0.2% PBST or PBS (3 times, 15 minutes each) and secondary antibodies/stains [donkey anti-rat IgG-Cy3 (1:500; Jackson ImmunoResearch #712-165-153), donkey anti-mouse IgG-Alexa-647 (1:500; Jackson ImmunoResearch #715-605-151), donkey anti-mouse Alexa-488 (1:500; Jackson ImmunoResearch #715-545-151), and/or Alexa-488 Phalloidin (1:1000; ThermoFisher A12379)] were applied in 0.2% PBST+NDS or PBS+NDS for 2 hours at room temperature. Tissues were further washed with 0.2% PBST or PBS and mounted in Vectashield with DAPI (Vector labs). Images were taken with LSM 710 Confocal Microscope (Zeiss).

Notch epistasis assay

UAS-Notch lines were crossed to either *nub-GAL4*, *UAS-CD8::mCherry* (control) or *nub-GAL4*, *UAS-amx*$^{\Delta ECD}$ flies. Wing discs from 3rd instar larvae were dissected out, fixed washed and stained for Cut as described earlier. Cut intensity within the wing pouch was quantified using ImageJ (https://imagej.nih.gov/ij/). Graph generation and statistical analysis was performed with GraphPad Prism software version 9.0. One way t-test was used to compare experiments. * = $p \leq 0.05$. **** = $p \leq 0.0001$.

MARCM analysis

The following fly lines were used for MARCM [51] analysis of *kuz* mutant clones:

hsFLP; tub-Gal80^{ts}, *FRT40A/CyO; tub-GAL4*, *UAS-GFP/TM6b*, *Tb* [102]

kuz^{e29-4}, *FRT40A/CyO* [50]

Flies were crossed and maintained at 25˚C. First-instar larvae (36–48 hours after egg laying) were heat shocked for 40 minutes twice a day at 37˚C. Wing discs were dissected in 1×PBS from wandering larvae (108–120 hours after egg laying). Discs were then fixed in 4% paraformaldehyde in PBS for 20 minutes at room temperature. Fixed discs were washed with 0.2% PBST. A mouse anti-Notch primary antibody (1:40; DSHB, C17.9C6, raised against the intracellular domain) was applied in 0.2% PBST with 5% NDS/0.1% NaN_3 overnight at 4˚C. Discs were further washed with 0.2% PBST after primary antibody staining. A donkey anti-mouse-Cy3 secondary antibody (1:500; Jackson ImmunoResearch #715-165-151) in 0.2% PBST was applied for 2 hours at room temperature. Stained discs were washed with 0.2% PBST and mounted with Vectashield with DAPI (Vector labs). Fluorescence Images were taken by LSM 710 Confocal Microscope (Zeiss).

Western blot of HA tagged Amx

To determine whether 3xHA::Amx is expressed in adult brains or ovaries, we performed western blot. Adult brains from *y*, *w; VK37{pattB-3xHA::amx}* flies were dissected out as described in [103]. For ovaries, we mated the *y*, *w; VK37{pattB-3xHA::amx}* females flies to male flies of the same genotype while supplying plenty of active yeast to stimulate oogenesis for two days prior to protein isolation. Ovaries were then dissected out from the abdomen in cold (4˚C) PBS. Dissected brains and ovaries were rinsed with cold PBS and placed immediately in cold 8M urea lysis buffer (8M urea, 10% glycerol, 0.5% SDS, 5% β-mercaptoethanol) with Halt Protease Inhibitor Cocktail 100X (Thermo Scientific, #78430) added before lysis. We homogenized the brains or ovaries were via pestle in 15 uL of 8M urea lysis buffer. Homogenate was incubated for 30 minutes on ice, and 2x Laemmli Sample Buffer (Bio-Rad, #1610737) was

added prior to gel loading. Best results were obtained when avoiding heating/boiling protein sample. Homogenate was loaded directly into Mini-PROTEAN TGX 4–20% Precast Gels (Bio-Rad, #4561094). SDS-PAGE (Sodium Dodecyl Sulphate–PolyAcrylamide Gel Electrophoresis) was run for 30 minutes at 120V in Tris/Glycine/SDS buffer (BioRad, #1610732). Protein was then transferred onto PVDF membrane using Bio-Rad TransBlot Turbo system using the low molecular weight protocol. The membrane was blocked with 5% skim milk in 0.5% Tween-20/Tris-Buffered Saline (TBST) for 1 hour at room temperature and then washed 3 times for 5 minutes with TBST. A primary antibody (rat anti-HA, 1:1,000, Sigma, 3F10) was diluted in 5% fetal bovine serum/TBST and the membrane was incubated overnight at 4˚C. The membrane was again washed with TBST and a secondary antibody (donkey anti-rat HRP, 1:5,000, Jackson ImmunoResearch, #712-035-150) was applied in 5% milk/TBST for 2 hours at room temperature. The membrane was washed again and imaged using SuperSignal West Femto Maximum Sensitivity Substrate (Thermo Scientific, 34096) and ChemiDoc imaging system (Bio-Rad) using default settings. The same protocol was used to compare the levels of overexpressed 3xHA::Amx^{FL} or 3xHA::Amx$^{\Delta ECD}$ from adult brains dissected from elav-GAL4/+; UAS-3xHA::Amx$^{FL\ or\ \Delta ECD}$ animals.

Longevity assay

To determine whether loss of *amx*, *amrt* or *bisc* causes lifespan defects, we compared the longevity of male flies that lack each gene (*amx*$^{\Delta}$, *amrt*$^{\Delta}$ or *bisc*$^{\Delta}$) to respective control flies in which the null allele has been rescued with genomic constructs (*VK37{amx}*, *VK37{amrt} or VK33{bisc*::*GFP}*). For *amx*, we also tested whether N'-3xHA tagged Amx (*y*, *w*, *amx*$^{\Delta}$*; VK37 {3xHA*::*amx}*) or human TM2D3 expressed under the control of fly *amx* regulatory elements (*y*, *w*, *amx*$^{\Delta}$*; VK37 {TM2D3}*) can also rescue the mutant phenotype. Flies were reared and collected as described in [104]. Ten animals were housed together in a single vial and flies were flipped to a new vial with fresh food every 2–3 days. Vials were kept in a 25˚C incubator with a 12 hr light/dark cycle. Dead flies were recorded after every vial flip. Generation of the Kaplan-Meier curve and statistical analysis was performed with GraphPad Prism 9.0. We applied log-rank test (Mantel-Cox), **** = $p \leq 0.0001$.

Climbing assay

8–10 flies that were age matched were placed in an empty vial and flies were tapped down to the bottom. The number of flies that successfully climbed past a 7 cm line from the bottom of the vial within 15 seconds were recorded. This was repeated 3 times for each group of flies. The graph was generated using GraphPad Prism 9.0.

Electrophysiological recordings of the giant fiber system

Electrophysiological recordings of the giant fiber system were performed with a protocol modified from [105]. Flies were first anesthetized on ice then transferred to a petri dish filled with soft dental wax; wings and legs were mounted in wax, ventral side down, using forceps. Five electrolytically sharpened tungsten electrodes were used: two for stimulating the giant fiber, one as a reference electrode, and two for recording from the TTM and DLM, respectively. To activate the giant fiber, two sharp tungsten electrodes were inserted into each eye and voltage stimulation was applied at different frequencies ranging from 0.5 Hz to 100 Hz. DLM and TTM responses were measured through the two electrodes implanted in the DLM and TTM.

For each adult fly, prior to applying high frequency stimulation on the giant fiber, low frequency stimulations at 0.5 Hz were applied after placing the two recording electrodes in TTM and DLM to ensure that the electrodes are recording from the proper muscles (the latency of

responses for TTM: 0.8 ms and for DLM: 1.2 ms [105]. For the actual experiments, high frequency train stimulations of 20 pulses were delivered to the giant fiber at 20, 50 and 100 Hz in random order. Ten times repetitive stimulations were applied for each particular frequency train, interspersed with few minutes rests between two trains of stimuli (for 20 Hz, 1 minute resting; 50 Hz 2 minutes and 100 Hz 3 minutes). 0.5 Hz stimulations were used again after high frequency stimulation to confirm that electrodes were still in the proper muscle. The aforementioned process was considered as one biological sample. Stimuli of the crossing electrodes were fixed at a duration of 10 microseconds at 10–13 V of amplitudes through a stimulus isolation unit (Digitimer Ltd, model DS2A) and the frequency of train stimuli was controlled by LabChart Pro-8 acquisition software (ADInstruments). A microelectrode amplifier (A-M system, Model 1800) was used for all recordings. PowerLab 4/35 (ADInstruments) was used for data acquisition. The probability of responses for one biological sample, under particular frequency of giant fiber stimulation, due to a particular stimulus, was calculated from the proportion of successful responses (out of 10) for both TTM and DLM pathways. The difference of 'probability of responses' between control and experimental samples (p-value) for each stimuli were calculated by multiple unpaired t-tests with Holm-Šídák correction for multiple comparisons using Graph Pad Prism 9.0. n.s. = not significant. * = $p \leq 0.05$. ** = $p \leq 0.01$. *** = $p \leq 0.001$. **** = $p \leq 0.0001$.

Supporting information

S1 Fig. *TM2D* genes are conserved in metazoan species. (A) Protein alignment of Human TM2D proteins across multiple species (human, mouse, frog, zebrafish, fly, worm). TM2 domain (red box, pfam05154) is highly conserved among the proteins and across species. C' terminus of the proteins are also well conserved across species. Black bars denote the regions that are commonly annotated as Signal Sequence, TMD (Transmembrane domain, #1), DRF or TMD (#2) in all human TM2D1-3 proteins (consensus regions) based on Uniprot (https://www.uniprot.org/). Gray bars show regions that have been annotated as Signal Sequence, TMD (#1) or TMD (#2) in one or two human TM2D1-3 proteins. (B-B') Phylogenetic analysis of TM2D family genes. (B) shows the phylogenetic tree based on UPGMA (unweighted pair group method with arithmetic mean) method, and (B') shows the tree based on the Neighbor-Joining method. In both cases, orthologs across different species are shown to be more closely related to each other than the three genes in each species.
(TIFF)

S2 Fig. *TM2D* null fly mutants do not express corresponding mRNAs. Reverse transcription followed by PCR (RT-PCR) to verify loss of *TM2D* gene transcripts in mutant fly lines. mRNA was isolated from animals homozygous for their respective alleles. (A) Single mutant lines lack their appropriate gene transcript while other *TM2D* transcripts are unaffected. (B) *amx amrt* double mutants express *bisc*. *TM2D* triple mutants lack all transcripts. *rp49* is a house-keeping gene used as a control for the reverse transcription reaction.
(TIFF)

S3 Fig. Epistasis experiments between $Amx^{\Delta ECD}$ and full-length Notch in the wing imaginal disc. (A) Overexpression of full-length Notch in the developing wing pouch via *nub-GAL4* causes a minor upregulation of Cut expression close to the wing margin, likely reflecting the availability of ligands within the wing pouch. (B) $Amx^{\Delta ECD}$ inhibits the increase of Cut expression induced by Notch as well as abolishing the normal expression levels of Cut, showing it is epistatic to full-length Notch. (C-D) Overexpression of NICD causes increased expression of Cut (green) (D-D"), compared to a control disc overexpressing LacZ, a neutral protein. (E)

Cut expression is about 5-fold higher in NICD expressing wing discs compared to control discs expressing LacZ. Scale bars = 50 μm in (A-D).
(TIFF)

S4 Fig. Truncated Amx causes wing notching or wing loss when expressed with multiple wing-expressed GAL4 drivers. (A) $Amx^{\Delta ECD}$ expressed in the developing wing pouch with *nub-GAL4* causes notching along the wing margin. (B) Homozygous *nub-GAL4*, *UAS-amx$^{\Delta ECD}$* recombinant animals show near complete loss of wing (arrow). (C) *dpp-GAL4* (expressed between the third and fourth wing veins) driven expression of Amx^{FL} has no effect on wing morphology. (D) *dpp-GAL4* driven expression of $Amx^{\Delta ECD}$ causes notching at the wing tip.
(TIFF)

S5 Fig. $Amx^{\Delta ECD}$ causes accumulation of Notch receptor at the cell cell surface. (A-C) Grey scale images of total Notch staining shown in Fig 5J'-L', revealing incresase in Notch levels upon overexpression of $Amx^{\Delta ECD}$ or *Psn* knockdown. (D-F") wing disc expressing LacZ (D-D"), $Amx^{\Delta ECD}$ (E-E") or *Psn-RNAi* (F-F") driven by *dpp-Gal4*. GAL4 expression domain is marked by mCherry (red) in D-F. Cell nuclei are marked by DAPI (blue) in D-F. Cell surface Notch is shown in rainbow in D'-F' or grey scale in D"-F". Notch accumulates at the cell surface upon of $Amx^{\Delta ECD}$ or *Psn* knockdown but to a lesser extent compared to total Notch staining. Scale bars = 5 μm in (A-C). Scale bars = 10 μm in (D-F).
(TIFF)

S6 Fig. *kuz* (ADAM10) null mutant clones do not show Notch accumulation. (A) $kuz^{-/-}$ clones (positively marked by GFP, green) were generated by MARCM using a heat shock induced Fippase (*hs-FLP*). The expression level and gross subcellular localization of Notch (magenta) is not altered in $kuz^{-/-}$ clones compared to control tissue (non-GFP cells). A" and A"' show the boxed region in A and A'. Scale bars = 50 μm.
(TIFF)

S7 Fig. $Amx^{\Delta ECD}$ is expressed at lower levels than Amx^{FL} and has a different subcellular localization pattern. (A) Western blot of Amx^{FL} and $Amx^{\Delta ECD}$ expression driven by pan-neuronal *elav-GAL4* driver. Expected band size for Amx^{FL} is 35 kDA. Expected band size for $Amx^{\Delta ECD}$ is 10 kDa. Since two bands are present around the expected size for $Amx^{\Delta ECD}$, both signals were quantified in (B). (B) $Amx^{\Delta ECD}$ expression is ~10x lower than Amx^{FL}. t-test. **** = $p<0.0001$. Error bars show SEM. (C-D) Immunostaining against HA tag (green) shows 3xHA::Amx^{FL} has a membranous expression pattern (C) compared to a more punctate pattern seen with 3xHA::$Amx^{\Delta ECD}$ (D). (E) RT-PCR on mRNA extracted from wing discs from control animals (genotype: *y w*) shows that all three *TM2D* genes are endogenously expressed in this tissue. Scale bars = 5 μm in (C-D).
(TIFF)

S8 Fig. *amrt* and *bisc* mutants show a shortened lifespan phenotype while amx mutants exhibit age-dependent climbing defects. (A-B) Lifespans of *amrt* and *bisc* mutants compared to their respective controls. Animals were reared at 25˚C; Log-rank test (Mantel-Cox), **** = $p<0.0001$. (A) $amrt^{\Delta}$ animals (dark yellow, n = 147) have reduced lifespan compared to $amrt^{\Delta}$ + *amrt* controls (pale dash yellow, n = 59). (B) $bisc^{\Delta}$ animals (dark pink, n = 94) have reduced lifespan compared to $bisc^{\Delta}$ + *bisc*::*GFP* controls (pale dash pink, n = 84). (C) amx^{Δ} mutants (on a *y w* mutant background) exhibit climbing defects that worsen over time compared to controls (*y w*). The absence or presence of the *white* gene does not affect this phenotype.
(TIFF)

S9 Fig. *amx* mRNA is expressed in nervous system of *Drosophila* according to transcriptomic databases. (A) Summary table for *amx* transcript expression provided by FlyAtlas (http://flyatlas.gla.ac.uk/FlyAtlas2/index.html?search=gene&gene=CG12127&idtype=cgnum#mobileTargetG). *amx* transcript is found in the Brain/CNS of adult flies, as well as other tissues. (B) Single-cell transcript data shows *amx* expressed in many but not all cells in the adult fly brain based on [53]. Clusters of cells positive for *repo* (glial marker) expression are circled in blue; the remaining cells are largely *elav* (neuronal marker) positive (https://scope.aertslab.org/). Red dots are cells positive for *amx* expression.
(TIFF)

S10 Fig. 3xHA::Amx expressed from a genomic rescue construct is detected in the *Drosophila* ovary and localizes to the cell membrane as well as intracellular puncta. (A-B) 3xHA::Amx (magenta) localizes to the plasma membrane (marked by Phalloidin, green) separating nurse cells (arrow heads). The signal is relatively low but clearly above background levels of *y w* control (A" vs. B"). The same membranous localization of HA staining is not seen in negative control (arrows). (C) Western blot on ovaries showing positive expression of 3xHA::Amx (lane 2, expected size 35 kDa) in amx^{Δ} flies compared to untagged Amx control in the same genetic background (lane 1); two ovary pairs were loaded per lane. Scale bars = 50 μm in (A-B).
(TIFF)

S11 Fig. Expression of 3xHA::Amx^{FL} cannot be detected through immunofluorescence staining of the adult brain. (A-B) Brains from ~1 week old animals carrying *3xHA*::amx^{FL} transgene (A) show no clear signal when immunostained for HA (green) compared to negative control (genotype: *y w*) brains (B). Scale bars = 50 μm in (A-B).
(TIFF)

S12 Fig. Giant fiber recordings from 5 day post eclosion flies stimulated at 20 and 50 Hz. (A,C). DLM muscles of 5 day old amx^{Δ} mutants (black) have a response similar to amx^{Δ} + *amx* controls (orange) at stimulation frequencies of 20 and 50 Hz. (B,D) TTM muscles show a small but significant decrease in response probability at 50 Hz but not 20 Hz. amx^{Δ} + *3xHA*::*amx* (blue) flies also perform as well as controls (A-D). Multiple unpaired t-tests with Holm-Šídák correction for multiple comparisons. * = $p<0.05$. Error bars show SEM.
(TIFF)

S13 Fig. Giant fiber recordings from 15 day post eclosion flies stimulated at 20, 50 and 100 Hz. (A,C,E) TTM failure rate at 20 and 50 Hz. Responses are similar between amx^{Δ} mutants (black) and amx^{Δ} + *amx* controls (orange) (A, C), with slight but significant failures were observed at 100 Hz (E). (B,D,F) DLM failure rate at 20 and 50 Hz. amx^{Δ} mutants have a response similar to amx^{Δ} + *amx* controls at 20 Hz (B) but begin to show significant failure to respond at 50 and 100 Hz (D,F). Multiple unpaired t-tests with Holm-Šídák correction for multiple comparisons. *** = $p<0.001$, **** = $p<0.0001$. Error bars show SEM.
(TIFF)

S14 Fig. Giant fiber recordings from 25 day post eclosion flies stimulated at 20 and 50 Hz. (A,C) TTM response at 20 and 50 Hz of 25 day old amx^{Δ} mutants is similar to controls and animals carrying a human *TM2D3* rescue construct. (B,D) At 25d old, amx^{Δ} mutants perform similarly to controls at 20 Hz (B) but show a significant increase in response failure at 50 Hz (D). Human *TM2D3* rescued flies again perform similarly to controls. Multiple unpaired t-tests with Holm-Šídák correction for multiple comparisons. * = $p<0.05$. ** = $p<0.01$, *** =

$p<0.001$. Error bars show SEM.
(TIFF)

S1 Table. Key resources used in this study. The following abbreviations are used. PMID: PubMed ID (https://pubmed.ncbi.nlm.nih.gov), BDSC: Bloomington Drosophila Stock Center ID (https://bdsc.indiana.edu), DSHB: Developmental Studies Hybridoma Bank ID (https://dshb.biology.uiowa.edu)
(DOCX)

S2 Table. Genotypes of the flies shown in each figure panel.
(DOCX)

Acknowledgments

We are grateful to Ms. Danqing Bei and Ms. Hongling Pan for performing *Drosophila* microinjections. We acknowledge the Knockout Mouse Phenotyping Project (KOMP2) and Internationational Mouse Phenotyping Consortium (IMPC) for the generation and phenotyping of *Tm2d1-3* knockout mouse strains. We thank Dr. Oguz Kanca for technical advice and useful suggestions. We thank Drs. Joshua Shulman, Hugo Bellen, Bart De Strooper, Katrien Horré, Motoo Kitagawa, Wataru Masuda, Kenji Matsuno and Tomoko Yamakawa for valuable discussions. We thank Ms. Shelley Gibson and Mr. J. Michael Harnish for helpful comments on the manuscript.

Author Contributions

Conceptualization: Jose L. Salazar, Sheng-An Yang, Shinya Yamamoto.

Data curation: Jose L. Salazar, Sheng-An Yang, Yong Qi Lin.

Formal analysis: Jose L. Salazar, Sheng-An Yang, Yong Qi Lin, Paul C. Marcogliese, Samantha L. Deal, Shinya Yamamoto.

Funding acquisition: Shinya Yamamoto.

Investigation: Jose L. Salazar, David Li-Kroeger, Samantha L. Deal.

Methodology: Jose L. Salazar, Yong Qi Lin, David Li-Kroeger, Paul C. Marcogliese, G. Gregory Neely, Shinya Yamamoto.

Project administration: Shinya Yamamoto.

Resources: David Li-Kroeger, Paul C. Marcogliese, Shinya Yamamoto.

Supervision: G. Gregory Neely, Shinya Yamamoto.

Validation: Jose L. Salazar, Sheng-An Yang, Yong Qi Lin, David Li-Kroeger, Samantha L. Deal, Shinya Yamamoto.

Visualization: Jose L. Salazar, Sheng-An Yang, Yong Qi Lin, Shinya Yamamoto.

Writing – original draft: Jose L. Salazar, Sheng-An Yang, Yong Qi Lin, David Li-Kroeger, Paul C. Marcogliese, Samantha L. Deal, G. Gregory Neely, Shinya Yamamoto.

Writing – review & editing: Jose L. Salazar, Sheng-An Yang, Shinya Yamamoto.

References

1. Long JM, Holtzman DM. Alzheimer Disease: An Update on Pathobiology and Treatment Strategies. Cell. Cell Press; 2019. pp. 312–339. https://doi.org/10.1016/j.cell.2019.09.001 PMID: 31564456

2. Sala Frigerio C, De Strooper B. Alzheimer's Disease Mechanisms and Emerging Roads to Novel Therapeutics. Annu Rev Neurosci. 2016; 39: 57–79. https://doi.org/10.1146/annurev-neuro-070815-014015 PMID: 27050320

3. Bellenguez C, Grenier-Boley B, Lambert JC. Genetics of Alzheimer's disease: where we are, and where we are going. Current Opinion in Neurobiology. Elsevier Ltd; 2020. pp. 40–48. https://doi.org/10.1016/j.conb.2019.11.024 PMID: 31863938

4. Karran E, Mercken M, Strooper B De. The amyloid cascade hypothesis for Alzheimer's disease: An appraisal for the development of therapeutics. Nature Reviews Drug Discovery. Nature Publishing Group; 2011. pp. 698–712. https://doi.org/10.1038/nrd3505 PMID: 21852788

5. Zhang S, Zhang M, Cai F, Song W. Biological function of Presenilin and its role in AD pathogenesis. Translational Neurodegeneration. BioMed Central; 2013. p. 15. https://doi.org/10.1186/2047-9158-2-15 PMID: 23866842

6. Kopan R, Ilagan MXG. The Canonical Notch Signaling Pathway: Unfolding the Activation Mechanism. Cell. 2009; 137: 216–233. https://doi.org/10.1016/j.cell.2009.03.045 PMID: 19379690

7. Artavanis-Tsakonas S, Matsuno K, Fortini ME. Notch signaling. Science (80-). 1995; 268: 225–232. https://doi.org/10.1126/science.7716513 PMID: 7716513

8. Cacace R, Sleegers K, Van Broeckhoven C. Molecular genetics of early-onset Alzheimer's disease revisited. Alzheimer's and Dementia. Elsevier Inc.; 2016. pp. 733–748. https://doi.org/10.1016/j.jalz.2016.01.012 PMID: 27016693

9. Goldman JS, Hahn SE, Catania JW, Larusse-Eckert S, Butson MB, Rumbaugh M, et al. Genetic counseling and testing for Alzheimer disease: Joint practice guidelines of the American College of Medical Genetics and the National Society of Genetic Counselors. Genet Med. 2011; 13: 597–605. https://doi.org/10.1097/GIM.0b013e31821d69b8 PMID: 21577118

10. Strittmatter WJ, Saunders AM, Schmechel D, Pericak-Vance M, Enghild J, Salvesen GS, et al. Apolipoprotein E: High-avidity binding to β-amyloid and increased frequency of type 4 allele in late-onset familial Alzheimer disease. Proc Natl Acad Sci U S A. 1993; 90: 1977–1981. https://doi.org/10.1073/pnas.90.5.1977 PMID: 8446617

11. Serrano-Pozo A, Das S, Hyman BT. APOE and Alzheimer's disease: advances in genetics, pathophysiology, and therapeutic approaches. The Lancet Neurology. Lancet Publishing Group; 2021. pp. 68–80. https://doi.org/10.1016/S1474-4422(20)30412-9 PMID: 33340485

12. Kunkle BW, Grenier-Boley B, Sims R, Bis JC, Damotte V, Naj AC, et al. Genetic meta-analysis of diagnosed Alzheimer's disease identifies new risk loci and implicates Aβ, tau, immunity and lipid processing. Nat Genet. 2019; 51: 414–430. https://doi.org/10.1038/s41588-019-0358-2 PMID: 30820047

13. Jakobsdottir J, van der Lee SJ, Bis JC, Chouraki V, Li-Kroeger D, Yamamoto S, et al. Rare Functional Variant in TM2D3 is Associated with Late-Onset Alzheimer's Disease. Haines JL, editor. PLOS Genet. 2016; 12: e1006327. https://doi.org/10.1371/journal.pgen.1006327 PMID: 27764101

14. Sim NL, Kumar P, Hu J, Henikoff S, Schneider G, Ng PC. SIFT web server: Predicting effects of amino acid substitutions on proteins. Nucleic Acids Res. 2012; 40: W452–W457. https://doi.org/10.1093/nar/gks539 PMID: 22689647

15. Adzhubei IA, Schmidt S, Peshkin L, Ramensky VE, Gerasimova A, Bork P, et al. A method and server for predicting damaging missense mutations. Nature Methods. Nat Methods; 2010. pp. 248–249. https://doi.org/10.1038/nmeth0410-248 PMID: 20354512

16. Kircher M, Witten DM, Jain P, O'roak BJ, Cooper GM, Shendure J. A general framework for estimating the relative pathogenicity of human genetic variants. Nat Genet. 2014; 46: 310–315. https://doi.org/10.1038/ng.2892 PMID: 24487276

17. Shannon MP. Characterization of the female-sterile mutant Almondex of Drosophila melanogaster. Genetica. 1972; 43: 244–256. https://doi.org/10.1007/BF00123632 PMID: 4625164

18. Shannon MP. The development of eggs produced by the female-sterile mutant almondex of Drosophila melanogaster. J Exp Zool. 1973; 183: 383–400. https://doi.org/10.1002/jez.1401830312 PMID: 4633255

19. Lehmann R, Jiménez F, Dietrich U, Campos-Ortega JA. On the phenotype and development of mutants of early neurogenesis in Drosophila melanogaster. Wilhelm Roux's Arch Dev Biol. 1983; 192: 62–74. https://doi.org/10.1007/BF00848482 PMID: 28305500

20. Lewis J. Neurogenic genes and vertebrate neurogenesis. Curr Opin Neurobiol. 1996; 6: 3–10. https://doi.org/10.1016/s0959-4388(96)80002-x PMID: 8794055

21. Salazar JL, Yamamoto S. Integration of Drosophila and human genetics to understand notch signaling related diseases. Advances in Experimental Medicine and Biology. Springer New York LLC; 2018. pp. 141–185. https://doi.org/10.1007/978-3-319-89512-3_8 PMID: 30030826

22. Cochran JN, McKinley EC, Cochran M, Amaral MD, Moyers BA, Lasseigne BN, et al. Genome sequencing for early-onset or atypical dementia: High diagnostic yield and frequent observation of multiple contributory alleles. Cold Spring Harb Mol Case Stud. 2019; 5. https://doi.org/10.1101/mcs.a003491 PMID: 31836585

23. Koenen A, Babendreyer A, Schumacher J, Pasqualon T, Schwarz N, Seifert A, et al. The DRF motif of CXCR6 as chemokine receptor adaptation to adhesion. PLoS One. 2017; 12. https://doi.org/10.1371/journal.pone.0173486 PMID: 28267793

24. Kajkowski EM, Lo CF, Ning X, Walker S, Sofia HJ, Wang W, et al. β-Amyloid Peptide-induced Apoptosis Regulated by a Novel Protein Containing a G Protein Activation Module. J Biol Chem. 2001; 276: 18748–18756. https://doi.org/10.1074/jbc.M011161200 PMID: 11278849

25. Michellod MA, Randsholt NB. Implication of the Drosophila beta-amyloid peptide binding-like protein AMX in Notch signaling during early neurogenesis. Brain Res Bull. 2008; 75: 305–309. https://doi.org/10.1016/j.brainresbull.2007.10.060 PMID: 18331889

26. Hori K, Sen A, Artavanis-Tsakonas S. Notch signaling at a glance. J Cell Sci. 2013; 126: 2135–2140. https://doi.org/10.1242/jcs.127308 PMID: 23729744

27. Duojia P, Rubin GM. Kuzbanian controls proteolytic processing of Notch and mediates lateral inhibition during Drosophila and vertebrate neurogenesis. Cell. 1997; 90: 271–280. https://doi.org/10.1016/s0092-8674(00)80335-9 PMID: 9244301

28. Mumm JS, Schroeter EH, Saxena MT, Griesemer A, Tian X, Pan DJ, et al. A ligand-induced extracellular cleavage regulates γ-secretase-like proteolytic activation of Notch1. Mol Cell. 2000; 5: 197–206. https://doi.org/10.1016/s1097-2765(00)80416-5 PMID: 10882062

29. De Strooper B, Annaert W, Cupers P, Saftig P, Craessaerts K, Mumm JS, et al. A presenilin-1-dependent γ-secretase-like protease mediates release of notch intracellular domain. Nature. 1999; 398: 518–522. https://doi.org/10.1038/19083 PMID: 10206645

30. Michellod M-A, Forquignon F, Santamaria P, Randsholt NB. Differential requirements for the neurogenic genealmondex duringDrosophila melanogaster development. genesis. 2003; 37: 113–122. https://doi.org/10.1002/gene.10233 PMID: 14595834

31. Bier E, Harrison MM, O'connor-Giles KM, Wildonger J. Advances in engineering the fly genome with the CRISPR-Cas system. Genetics. 2018; 208: 1–18. https://doi.org/10.1534/genetics.117.1113 PMID: 29301946

32. Knott GJ, Doudna JA. CRISPR-Cas guides the future of genetic engineering. Science. American Association for the Advancement of Science; 2018. pp. 866–869. https://doi.org/10.1126/science.aat5011 PMID: 30166482

33. Li-Kroeger D, Kanca O, Lee PT, Cowan S, Lee MT, Jaiswal M, et al. An expanded toolkit for gene tagging based on MiMIC and scarless CRISPR tagging in Drosophila. Elife. 2018; 7. https://doi.org/10.7554/eLife.38709 PMID: 30091705

34. Schweisguth F. Asymmetric cell division in the Drosophila bristle lineage: From the polarization of sensory organ precursor cells to Notch-mediated binary fate decision. Wiley Interdiscip Rev Dev Biol. 2015; 4: 299–309. https://doi.org/10.1002/wdev.175 PMID: 25619594

35. Córdoba S, Estella C. Role of Notch Signaling in Leg Development in Drosophila melanogaster. Advances in Experimental Medicine and Biology. Springer; 2020. pp. 103–127. https://doi.org/10.1007/978-3-030-34436-8_7 PMID: 32060874

36. Sarov M, Barz C, Jambor H, Hein MY, Schmied C, Suchold D, et al. A genome-wide resource for the analysis of protein localisation in Drosophila. Elife. 2016; 5. https://doi.org/10.7554/eLife.12068 PMID: 26896675

37. Chintapalli VR, Wang J, Dow JAT. Using FlyAtlas to identify better Drosophila melanogaster models of human disease. Nature Genetics. Nature Publishing Group; 2007. pp. 715–720. https://doi.org/10.1038/ng2049 PMID: 17534367

38. Brown JB, Boley N, Eisman R, May GE, Stoiber MH, Duff MO, et al. Diversity and dynamics of the Drosophila transcriptome. Nature. 2014; 512: 393–399. https://doi.org/10.1038/nature12962 PMID: 24670639

39. Li H, Janssens J, De Waegeneer M, Saroja Kolluru S, Davie K, Gardeux V, et al. Fly Cell Atlas: a single-cell transcriptomic atlas of the adult fruit fly. bioRxiv. 2021; 2021.07.04.451050. https://doi.org/10.1101/2021.07.04.451050

40. Brand AH, Perrimon N. Targeted gene expression as a means of altering cell fates and generating dominant phenotypes. Development. 1993; 118. PMID: 8223268

41. Housden BE, Millen K, Bray SJ. Drosophila reporter vectors compatible with φC31 integrase transgenesis techniques and their use to generate new notch reporter fly lines. G3 Genes, Genomes, Genet. 2012; 2: 79–82. https://doi.org/10.1534/g3.111.001321 PMID: 22384384

42. Micchelli CA, Rulifson EJ, Blair SS. The function and regulation of cut expression on the wing margin of Drosophila: Notch, Wingless and a dominant negative role for Delta and Serrate. Development. 1997; 124: 1485–1495. PMID: 9108365

43. Venken KJT, He Y, Hoskins RA, Bellen HJ. P[acman]: A BAC transgenic platform for targeted insertion of large DNA fragments in D. melanogaster. Science (80-). 2006; 314: 1747–1751. https://doi.org/10.1126/science.1134426 PMID: 17138868

44. Bischof J, Björklund M, Furger E, Schertel C, Taipale J, Basler K. A versatile platform for creating a comprehensive UAS-ORFeome library in Drosophila. Dev. 2012; 140: 2434–2442. https://doi.org/10.1242/dev.088757 PMID: 23637332

45. Lieber T, Kidd S, Young MW. Kuzbanian-mediated cleavage of Drosophila Notch. Genes Dev. 2002; 16: 209–221. https://doi.org/10.1101/gad.942302 PMID: 11799064

46. Doherty D, Feger G, Younger-Shepherd S, Jan LY, Jan YN. Delta is a ventral to dorsal signal complementary to Serrate, another notch ligand, in Drosophila wing formation. Genes Dev. 1996; 10: 421–434. https://doi.org/10.1101/gad.10.4.421 PMID: 8600026

47. Fehon RG, Kooh PJ, Rebay I, Regan CL, Xu T, Muskavitch MAT, et al. Molecular interactions between the protein products of the neurogenic loci Notch and Delta, two EGF-homologous genes in Drosophila. Cell. 1990; 61: 523–534. https://doi.org/10.1016/0092-8674(90)90534-l PMID: 2185893

48. Kang J, Shin S, Perrimon N, Shen J. An evolutionarily conserved role of presenilin in neuronal protection in the aging drosophila brain. Genetics. 2017; 206: 1479–1493. https://doi.org/10.1534/genetics.116.196881 PMID: 28495961

49. Vaccari T, Lu H, Kanwar R, Fortini ME, Bilder D. Endosomal entry regulates Notch receptor activation in Drosophila melanogaster. J Cell Biol. 2008; 180: 755–762. https://doi.org/10.1083/jcb.200708127 PMID: 18299346

50. Rooke J, Pan D, Xu T, Rubin GM. KUZ, a conserved metalloprotease-disintegrin protein with two roles in Drosophila neurogenesis. Science (80-). 1996; 273: 1227–1231. https://doi.org/10.1126/science.273.5279.1227 PMID: 8703057

51. Lee T, Luo L. Mosaic analysis with a repressible neurotechnique cell marker for studies of gene function in neuronal morphogenesis. Neuron. 1999; 22: 451–461. https://doi.org/10.1016/s0896-6273(00)80701-1 PMID: 10197526

52. Flatt T. Survival costs of reproduction in Drosophila. Exp Gerontol. 2011; 46: 369–375. https://doi.org/10.1016/j.exger.2010.10.008 PMID: 20970491

53. Davie K, Janssens J, Koldere D, De Waegeneer M, Pech U, Kreft Ł, et al. A Single-Cell Transcriptome Atlas of the Aging Drosophila Brain. Cell. 2018; 174: 982–998.e20. https://doi.org/10.1016/j.cell.2018.05.057 PMID: 29909982

54. Pauli A, Althoff F, Oliveira RA, Heidmann S, Schuldiner O, Lehner CF, et al. Cell-Type-Specific TEV Protease Cleavage Reveals Cohesin Functions in Drosophila Neurons. Dev Cell. 2008; 14: 239–251. https://doi.org/10.1016/j.devcel.2007.12.009 PMID: 18267092

55. Kreko-Pierce T, Azpurua J, Mahoney RE, Eaton BA. Extension of health span and life span in Drosophila by S107 requires the calstabin homologue FK506-BP2. J Biol Chem. 2016; 291: 26045–26055. https://doi.org/10.1074/jbc.M116.758839 PMID: 27803160

56. Allen MJ, Godenschwege TA. Electrophysiological recordings from the Drosophila giant fiber system (GFS). Cold Spring Harb Protoc. 2010; 5: pdb.prot5453. https://doi.org/10.1101/pdb.prot5453 PMID: 20647357

57. Oyston LJ, Lin YQ, Khuong TM, Wang Q-P, Lau MT, Clark T, et al. Neuronal Lamin regulates motor circuit integrity and controls motor function and lifespan. Cell Stress. 2018; 2: 225–232. https://doi.org/10.15698/cst2018.09.152 PMID: 31225490

58. Martinez VG, Javadi CS, Ngo E, Ngo L, Lagow RD, Zhang B. Age-related changes in climbing behavior and neural circuit physiology in Drosophila. Dev Neurobiol. 2007; 67: 778–791. https://doi.org/10.1002/dneu.20388 PMID: 17443824

59. Das P, Salazar JL, Li-Kroeger D, Yamamoto S, Nakamura M, Sasamura T, et al. Maternal almondex, a neurogenic gene, is required for proper subcellular Notch distribution in early Drosophila embryogenesis. Dev Growth Differ. 2020; 62: 80–93. https://doi.org/10.1111/dgd.12639 PMID: 31782145

60. The Kasahara M. 2R hypothesis: an update. Current Opinion in Immunology. Curr Opin Immunol; 2007. pp. 547–552. https://doi.org/10.1016/j.coi.2007.07.009 PMID: 17707623

61. Glasauer SMK, Neuhauss SCF. Whole-genome duplication in teleost fishes and its evolutionary consequences. Molecular Genetics and Genomics. Springer Verlag; 2014. pp. 1045–1060. https://doi.org/10.1007/s00438-014-0889-2 PMID: 25092473

62. Lee Y, Chang DJ, Lee YS, Chang KA, Kim H, Yoon JS, et al. β-amyloid peptide binding protein does not couple to G protein in a heterologous Xenopus expression system. J Neurosci Res. 2003; 73: 255–259. https://doi.org/10.1002/jnr.10652 PMID: 12836168

63. Yamamoto S, Schulze KL, Bellen HJ. Introduction to notch signaling. Methods in Molecular Biology. Humana Press Inc.; 2014. pp. 1–14. https://doi.org/10.1007/978-1-4939-1139-4_1

64. Artavanis-Tsakonas S, Muskavitch MAT. Notch: The past, the present, and the future. Current Topics in Developmental Biology. 2010. https://doi.org/10.1016/S0070-2153(10)92001-2

65. Lehmann R, Dietrich U, Jiménez F, Campos-Ortega JA. Mutations of early neurogenesis in Drosophila. Wilhelm Roux's Arch Dev Biol. 1981; 190: 226–229. https://doi.org/10.1007/BF00848307 PMID: 28305572

66. Larkin A, Marygold SJ, Antonazzo G, Attrill H, Dos Santos G, Garapati P V., et al. FlyBase: updates to the Drosophila melanogaster knowledge base. Nucleic Acids Res. 2021; 49: D899–D907. https://doi.org/10.1093/nar/gkaa1026 PMID: 33219682

67. Oughtred R, Rust J, Chang C, Breitkreutz BJ, Stark C, Willems A, et al. The BioGRID database: A comprehensive biomedical resource of curated protein, genetic, and chemical interactions. Protein Sci. 2021; 30: 187–200. https://doi.org/10.1002/pro.3978 PMID: 33070389

68. Huttlin EL, Bruckner RJ, Paulo JA, Cannon JR, Ting L, Baltier K, et al. Architecture of the human interactome defines protein communities and disease networks. Nature. 2017; 545: 505–509. https://doi.org/10.1038/nature22366 PMID: 28514442

69. Haney MS, Bohlen CJ, Morgens DW, Ousey JA, Barkal AA, Tsui CK, et al. Identification of phagocytosis regulators using magnetic genome-wide CRISPR screens. Nat Genet. 2018; 50: 1716–1727. https://doi.org/10.1038/s41588-018-0254-1 PMID: 30397336

70. Zhang Y, Chen K, Sloan SA, Bennett ML, Scholze AR, O'Keeffe S, et al. An RNA-sequencing transcriptome and splicing database of glia, neurons, and vascular cells of the cerebral cortex. J Neurosci. 2014; 34: 11929–11947. https://doi.org/10.1523/JNEUROSCI.1860-14.2014 PMID: 25186741

71. Dickinson ME, Flenniken AM, Ji X, Teboul L, Wong MD, White JK, et al. High-throughput discovery of novel developmental phenotypes. Nature. 2016; 537: 508–514. https://doi.org/10.1038/nature19356 PMID: 27626380

72. Guo Y, Livne-Bar I, Zhou L, Boulianne GL. Drosophila presenilin is required for neuronal differentiation and affects notch subcellular localization and signaling. J Neurosci. 1999; 19: 8435–8442. https://doi.org/10.1523/JNEUROSCI.19-19-08435.1999 PMID: 10493744

73. Watson MR, Lagow RD, Xu K, Zhang B, Bonini NM. A Drosophila model for amyotrophic lateral sclerosis reveals motor neuron damage by human SOD1. J Biol Chem. 2008; 283: 24972–24981. https://doi.org/10.1074/jbc.M804817200 PMID: 18596033

74. Luan Z, Reddig K, Li HS. Loss of Na+/K+-ATPase in Drosophila photoreceptors leads to blindness and age-dependent neurodegeneration. Exp Neurol. 2014; 261: 791–801. https://doi.org/10.1016/j.expneurol.2014.08.025 PMID: 25205229

75. Zhao XL, Wang WA, Tan JX, Huang JK, Zhang X, Zhang BZ, et al. Expression of β-amyloid induced age-dependent presynaptic and axonal changes in Drosophila. J Neurosci. 2010; 30: 1512–1522. https://doi.org/10.1523/JNEUROSCI.3699-09.2010 PMID: 20107079

76. Hampel H, Mesulam MM, Cuello AC, Farlow MR, Giacobini E, Grossberg GT, et al. The cholinergic system in the pathophysiology and treatment of Alzheimer's disease. Brain. Oxford University Press; 2018. pp. 1917–1933. https://doi.org/10.1093/brain/awy132 PMID: 29850777

77. Feng R, Wang H, Wang J, Shrom D, Zeng X, Tsien JZ. Forebrain degeneration and ventricle enlargement caused by double knockout of Alzheimer's presenilin-1 and presenilin-2. Proc Natl Acad Sci U S A. 2004; 101: 8162–8167. https://doi.org/10.1073/pnas.0402733101 PMID: 15148382

78. Saura CA, Choi SY, Beglopoulos V, Malkani S, Zhang D, Rao BSS, et al. Loss of presenilin function causes impairments of memory and synaptic plasticity followed by age-dependent neurodegeneration. Neuron. 2004; 42: 23–36. https://doi.org/10.1016/s0896-6273(04)00182-5 PMID: 15066262

79. Tabuchi K, Chen G, Südhof TC, Shen J. Conditional forebrain inactivation of nicastrin causes progressive memory impairment and age-related neurodegeneration. J Neurosci. 2009; 29: 7290–301. https://doi.org/10.1523/JNEUROSCI.1320-09.2009 PMID: 19494151

80. Wines-Samuelson M, Schulte EC, Smith MJ, Aoki C, Liu X, Kelleher RJ, et al. Characterization of age-dependent and progressive cortical neuronal degeneration in Presenilin conditional mutant mice. PLoS One. 2010; 5: 10195. https://doi.org/10.1371/journal.pone.0010195 PMID: 20419112

81. Watanabe H, Iqbal M, Zheng J, Wines-Samuelson M, Shen J. Partial loss of presenilin impairs age-dependent neuronal survival in the cerebral cortex. J Neurosci. 2014; 34: 15912–15922. https://doi.org/10.1523/JNEUROSCI.3261-14.2014 PMID: 25429133

82. Salazar JL, Yang S-A, Yamamoto S. Post-developmental roles of notch signaling in the nervous system. Biomolecules. 2020; 10. https://doi.org/10.3390/biom10070985 PMID: 32630239

83. Zhang C, Wu B, Beglopoulos V, Wines-Samuelson M, Zhang D, Dragatsis I, et al. Presenilins are essential for regulating neurotransmitter release. Nature. 2009; 460: 632–636. https://doi.org/10.1038/nature08177 PMID: 19641596

84. Wu B, Yamaguchi H, Lai FA, Shen J. Presenilins regulate calcium homeostasis and presynaptic function via ryanodine receptors in hippocampal neurons. Proc Natl Acad Sci U S A. 2013; 110: 15091–15096. https://doi.org/10.1073/pnas.1304171110 PMID: 23918386

85. Fu R, Shen Q, Xu P, Luo JJ, Tang Y. Phagocytosis of microglia in the central nervous system diseases. Mol Neurobiol. 2014; 49: 1422–1434. https://doi.org/10.1007/s12035-013-8620-6 PMID: 24395130

86. Etchegaray JI, Elguero EJ, Tran JA, Sinatra V, Feany MB, McCall K. Defective phagocytic corpse processing results in neurodegeneration and can be rescued by TORC1 activation. J Neurosci. 2016; 36: 3170–3183. https://doi.org/10.1523/JNEUROSCI.1912-15.2016 PMID: 26985028

87. Hakim-Mishnaevski K, Flint-Brodsly N, Shklyar B, Levy-Adam F, Kurant E. Glial Phagocytic Receptors Promote Neuronal Loss in Adult Drosophila Brain. Cell Rep. 2019; 29: 1438–1448.e3. https://doi.org/10.1016/j.celrep.2019.09.086 PMID: 31693886

88. Schnute B, Troost T, Klein T. Endocytic trafficking of the notch receptor. Advances in Experimental Medicine and Biology. Springer New York LLC; 2018. pp. 99–122. https://doi.org/10.1007/978-3-319-89512-3_6 PMID: 30030824

89. Yamamoto S, Charng WL, Bellen HJ. Endocytosis and intracellular trafficking of notch and its ligands. Current Topics in Developmental Biology. Curr Top Dev Biol; 2010. https://doi.org/10.1016/S0070-2153(10)92005-X PMID: 20816395

90. Baron M. Endocytic routes to Notch activation. Seminars in Cell and Developmental Biology. Elsevier Ltd; 2012. pp. 437–442. https://doi.org/10.1016/j.semcdb.2012.01.008 PMID: 22285298

91. Fortini ME, Bilder D. Endocytic regulation of Notch signaling. Current Opinion in Genetics and Development. NIH Public Access; 2009. pp. 323–328. https://doi.org/10.1016/j.gde.2009.04.005 PMID: 19447603

92. Melcarne C, Lemaitre B, Kurant E. Phagocytosis in Drosophila: From molecules and cellular machinery to physiology. Insect Biochem Mol Biol. 2019; 109: 1–12. https://doi.org/10.1016/j.ibmb.2019.04.002 PMID: 30953686

93. Bischof J, Maeda RK, Hediger M, Karch F, Basler K. An optimized transgenesis system for Drosophila using germ-line-specific φC31 integrases. Proc Natl Acad Sci U S A. 2007; 104: 3312–3317. https://doi.org/10.1073/pnas.0611511104 PMID: 17360644

94. Port F, Chen HM, Lee T, Bullock SL. Optimized CRISPR/Cas tools for efficient germline and somatic genome engineering in Drosophila. Proc Natl Acad Sci U S A. 2014; 111: E2967–E2976. https://doi.org/10.1073/pnas.1405500111 PMID: 25002478

95. Housden BE, Perrimon N. Design and generation of donor constructs for genome engineering in Drosophila. Cold Spring Harb Protoc. 2016; 2016: 789–793. https://doi.org/10.1101/pdb.prot090787 PMID: 27587780

96. Li J, Housden BE, Bray SJ. Notch signaling assays in Drosophila cultured cell lines. Methods Mol Biol. 2014; 1187: 131–141. https://doi.org/10.1007/978-1-4939-1139-4_10 PMID: 25053486

97. Wharton KA, Johansen KM, Xu T, Artavanis-Tsakonas S. Nucleotide sequence from the neurogenic locus Notch implies a gene product that shares homology with proteins containing EGF-like repeats. Cell. 1985; 43: 567–581. https://doi.org/10.1016/0092-8674(85)90229-6 PMID: 3935325

98. Harnish J, Deal SL, Chao HT, Wangler MF, Yamamoto S. In vivo functional study of disease-associated rare human variants using drosophila. J Vis Exp. 2019; 2019. https://doi.org/10.3791/59658 PMID: 31498321

99. Marcogliese PC, Shashi V, Spillmann RC, Stong N, Rosenfeld JA, Koenig MK, et al. IRF2BPL Is Associated with Neurological Phenotypes. Am J Hum Genet. 2018; 103: 245–260. https://doi.org/10.1016/j.ajhg.2018.07.006 PMID: 30057031

100. O'Neill EM, Rebay I, Tjian R, Rubin GM. The activities of two Ets-related transcription factors required for drosophila eye development are modulated by the Ras/MAPK pathway. Cell. 1994; 78: 137–147. https://doi.org/10.1016/0092-8674(94)90580-0 PMID: 8033205

101. Yamamoto S, Charng WL, Rana NA, Kakuda S, Jaiswal M, Bayat V, et al. A mutation in EGF repeat-8 of notch discriminates between serrate/jagged and delta family ligands. Science (80-). 2012; 338: 1229–1232. https://doi.org/10.1126/science.1228745 PMID: 23197537

102. Yang SA, Deng WM. Serrate/notch signaling regulates the size of the progenitor cell pool in Drosophila imaginal rings. Genetics. 2018; 209: 829–843. https://doi.org/10.1534/genetics.118.300963 PMID: 29773559

103. Tito AJ, Cheema S, Jiang M, Zhang S. A simple one-step dissection protocol for whole-mount preparation of adult drosophila brains. J Vis Exp. 2016; 2016: 55128. https://doi.org/10.3791/55128 PMID: 27929474

104. Linford NJ, Bilgir C, Ro J, Pletcher SD. Measurement of lifespan in Drosophila melanogaster. J Vis Exp. 2013 [cited 4 Mar 2021]. https://doi.org/10.3791/50068 PMID: 23328955

105. Tanouye MA, Wyman RJ. Motor outputs of giant nerve fiber in Drosophila. J Neurophysiol. 1980; 44: 405–421. https://doi.org/10.1152/jn.1980.44.2.405 PMID: 6774064